Manuscript prepared for Atmos. Meas. Tech.
with version 2014/07/29 7.12 Copernicus papers of the LaTeX class copernicus.cls.
Date: 7 December 2015

Interannual variability of temperature in the UTLS region over Ganges-Brahmaputra-Meghna basin based on COSMIC GNSS RO data

Khandu [a], Joseph Awange[a,b,c], and Ehsan Forootan[d]

[a]Depart of Spatial Sciences, Curtin University, Perth, Australia
[b]Geodetic Institute, Karlsruhe University of Technology (KIT), Karlsruhe, Germany
[c]Department of Geophysics, Kyoto University, Kyoto Japan
[d]Institute of Geodesy and Geoinformation, Bonn University, Bonn, Germany

Correspondence to: Khandu (khandu@postgrad.curtin.edu.au)

Abstract. Poor reliability of radiosonde records across South Asia imposes serious challenges in understanding the structure of upper-tropospheric and lower-stratospheric (UTLS) region. The Constellation Observing System for Meteorology, Ionosphere, and Climate (COSMIC) mission launched in April 2006 have overcome many observational limitations inherent in conventional atmospheric sounding instruments. We examined interannual variability of UTLS temperature over the Ganges-Brahmaputra-Meghna (GBM) basin in South Asia using monthly accumulated COSMIC radio occultation (RO) data, together with two global reanalysis products. Comparisons between August 2006 and December 2013 indicated that MERRA (Modern-Era Retrospective Analysis for Research Application) and ERA-Interim (European Centre for Medium-Range Weather Forecasts reanalysis) were warmer by 2°C between 200 hPa and 50 hPa but these warm bias was found to be consistent over time resulting in a relative bias of ±0.5°C. The UTLS temperature showed considerable interannual variability from 2006-2013 in addition to warming (cooling) trends in the troposphere (stratosphere). The cold (warm) anomalies in the upper troposphere (tropopause region) was associated with warm ENSO (El Niño Southern Oscillation) phase while stratospheric sudden warming (SSW) signals were seen in stratospheric temperature anomalies. The tropopause also indicated considerable seasonal variability with its height reaching as high as 18.5 km during the peak monsoon period. PCA (Principal Component Analysis) decomposition of tropopause temperatures and heights over the basin showed ENSO accounts for 73% of the interannual variability with a correlation of 0.77 with Niño3.4 index whereas the quasi-biennial oscillation (QBO) explains about 10% of the variability. The largest tropopause anomaly associated with ENSO occurred during winter, when ENSO was at its peak. The largest anomaly was recorded during the last major El Niño event of 2009/2010, where tropopause temperature (height) increased (decreased) by about 1.5°C (300 me-

ters). In general, we observed a decreasing (increasing) trend in tropopause temperature (height) during the last 8 years.

1 Introduction

The upper troposphere lower stratosphere (UTLS) region (400 hPa - 30 hPa) is characterised by step changes in static stability (temperature lapse rate) with large gradients in a number of radiatively active trace gases, including ozone and water vapour (Reid and Gage, 1985; Randel et al., 2000). The variability and changes in temperature of the UTLS region plays an important role in regulating the exchange of water vapour, ozone, and other trace gases between the troposphere and the stratosphere, which is important for the dynamical and radiative balance of the atmosphere. Observational evidences from balloon-borne radiosondes (1950 onwards) and satellite-based measurements (1979 onwards) suggest that the troposphere has warmed considerably over the past decades with substantial cooling in the lower stratosphere (Karl et al., 2006; Bindoff et al., 2013; Lott et al., 2013; Thorne et al., 2013). Much of this temperature changes has been attributed to the anthropogenic emissions of the well-mixed greenhouse gases, which are consistent with trends from climate model simulations (e.g., Lott et al., 2013; Santer et al., 2008). The *tropopause*, which marks the separation between the two boundary layers in the UTLS region is of special importance for understanding the transport of water vapour into the stratosphere and exchange of ozone between the two layers (Randel et al., 2000). On the other hand, the height of the tropopause is affected by the heat balance of both the troposphere and the stratosphere. For instance, warming of the troposphere due to increasing green house gas concentrations raises the tropopause. Thus, changes in the height of the tropopause provide a sensitive indicator of climate change including human effects on climate (Santer et al., 2003a, b, 2008).

While there are increasing evidences in the recent changes in the vertical structure of the UTLS region including warming (cooling) troposphere (stratosphere) and ozone depletion (see, e.g., Bindoff et al., 2013; Lott et al., 2013), large observational uncertainties still exists in radiosonde measurements over the South Asian continent (specifically over India), which has been highlighted over the years (e.g., Das Gupta et al., 2005; Sun et al., 2010; Kumar et al., 2011; Ansari et al., 2015). Previous studies have reported anomalously large warm biases in radiosonde observations over India and some stations have been recently updated by the Indian Meteorological Department (IMD) with Global Positioning System (GPS)-based radiosondes to improve their observational skills (see, Kumar et al., 2011). Ansari et al. (2015) reported that GPS-based radiosonde temperature data have improved by many-fold from a bias of 2.6-5.0°C to -0.1-0.1°C. However, our analysis based on 18 radiosondes (15 conventional and 3 GPS-based sondes) over India from August 2006 to December 2013 showed that GPS-based radiosondes still exhibited large warm biases against the COSMIC RO data and anomalously high variations in the UTLS region. The biases were however found to be re-

duced by more than half from 2.72°C to 1.20°C. As a result, trends in upper air temperatures might be of limited quality, thus, affecting the climate change attribution studies over the region (Seidel et al., 2011; Steiner et al., 2011).

In order to improve on these limitations, a more robust space-based technique known as the *Global Navigation Satellite System (GNSS) radio occultation (RO)* (e.g., Melbourne et al., 1994; Ware et al., 1996; Kursinski et al., 1997; Awange, 2012) has emerged as an important climate monitoring system over the past decade (see e.g., Anthes, 2011, and reference therein). GNSS RO technique utilises the time delay information of the occulted GNSS signals, which passes through the atmosphere and is received by Low Earth Orbiting (LEO) satellites. The primary observables are GNSS phase path and signal amplitude, which can be subsequently converted into atmospheric profiles (of e.g., refractivity, temperature) using the assumption of spherical geometry of refractivity (e.g., Melbourne et al., 1994; Rocken et al., 1997). Nowadays, the retrieved bending angles can be directly applied in climate- and weather-related studies, thereby introducing less uncertainty in the observation system (see, e.g., Lewis, 2009; Schmidt et al., 2010). The use of GNSS RO data is advantageous since it provides 24-hour global coverage, high vertical resolution, and highly accurate profiles of the UTLS region (see., e.g., Sun et al., 2010; Khandu et al., 2011). Several studies have demonstrated the usefulness of GNSS RO in improving numerical weather prediction (NWP) forecasts (e.g., Healy and Thépaut, 2006; Cucurull et al., 2007; Poli et al., 2008, 2010), climate studies (Foelsche et al., 2008; Schmidt et al., 2010; Steiner et al., 2013) and space weather/ionospheric research and operations (e.g., Lee et al., 2012; Zhang et al., 2014) over the past two decades. The number of RO profiles has increased substantially over the past years with the launch of several GNSS RO missions enabling wider applications in regional studies (see, e.g., Anthes, 2011). For instance, the joint Taiwan-US mission Constellation Observing System for Meteorology, Ionosphere, and Climate (COSMIC)/FORMOSA Satellite Mission 3 (COSMIC/FORMOSAT-3, hereafter, COSMIC) (Anthes et al., 2008) has recorded about 1500 RO soundings per day globally with 70-90% of the soundings reaching within one km of the Earth's surface since August 2006.

Several studies have analyzed the long-term variations of temperature in the UTLS region such as annual, monthly, seasonal, and interannual variations using observations from global network of radiosondes, satellite-based measurements, and global reanalysis including the various aspects of tropopause characteristics (e.g., Reid and Gage, 1985; Randel et al., 2000; Gettelman et al., 2001; Gettelman and de F. Foster, 2002; Santer et al., 2003a, b; Seidel and Randel, 2006; Wilcox et al., 2011; Lott et al., 2013). Large-scale temporal variability of the tropopause is dominated by an annual cycle and longer-term interannual variability associated with large-scale ocean-atmospheric circulation phenomenon such as El Nino Southern Oscillation (ENSO, Trenberth, 1990) and stratospheric zonal wind variations, also known as quasi-biennial oscillation (QBO, Baldwin et al., 2001). The ENSO mode is depicted as a dumbbell pattern in the central Pacific (Randel et al., 2000; Gettelman et al., 2001) while QBO mode is a symmetrical structure across the equator (Randel et al., 2000).

Over the Indian monsoon region, Kulkarni and Verma (1993) found that the composites of mean tropopause height was significantly higher for good monsoon years, which coincides with the cold ENSO events. With the increasing record of GNSS RO record both in time and space, it is now possible to infer decadal temperature trends in the UTLS region and the tropopause with a structural uncertainty of less than 0.06°C in the tropics and mid-latitudes (Steiner et al., 2013). Based on the approximately 9 years of GNSS RO data from CHAllenging Minisatellite Payload (CHAMP, 2001-2008 Wickert et al., 2001), Gravity Recovery And Climate Experiment (GRACE, 2006-2009 Wickert et al., 2009) and COSMIC (2006-2009), Schmidt et al. (2010) found an increase of global tropopause height (5-9 m/year) with an upper tropospheric warming and a lower stratospheric cooling. In general, the tropopause height variations are positively (negatively) correlated with upper tropospheric (lower stratospheric) temperature variations.

From the hydrological perspective, the Ganges-Brahmaputra-Meghna (GBM) river basin in South Asia is a complex region consisting of the Himalayas (in the north) and vast alluvial flood plains (in the south) and and also consists of the world's third largest freshwater outlet (Chowdhury and Ward, 2004). The highly seasonal southwest Indian monsoon lasts from June to September with the rest of the period remaining relatively dry. While short-term variations in monsoon are associated with deep convective activities and horizontal advection through cold trap regions, modulation by equatorial planetary waves (e.g., Mehta et al., 2010), long-term variations are modulated by ENSO and the Indian Ocean Dipole (IOD, Saji et al., 1999) mode, another large-scale coupled ocean and atmosphere phenomenon in equatorial Indian ocean. The two modes (ENSO and IOD) generally have opposite effects over the region in terms of the precipitation with lower than normal rainfall during warm ENSO phase (also called El Niño) and higher than normal rainfall during positive IOD events (e.g., Ashok and Saji, 2007; Krishnamurti et al., 2013). The surface air temperature was found to be warmer in summer during El Niño events while winter and spring surface temperatures were found to be mainly induced by Indian Ocean sea surface temperature (SST) anomalies (Chowdary et al., 2014). Although relatively new, it is likely that IOD mode may have a significant impact on the variability of temperature in the UTLS region due to their significance on the regional atmospheric process. Previous studies have suggested that tropopause heights could be used as an additional indicator of Indian monsoon due to its high correlation with rainfall in May (Kulkarni and Verma, 1993). The rising mountains along the southern foothills of the Himalayas act as barriers to the Indian monsoon generating deep convection along the Himalayan fronts, which may affect the spatial variability of tropopause parameters such as temperatures and heights. The growing population and expanding industrialisation in and around the GBM basin are the major source of atmospheric pollution and greenhouse gases (GHGs), and a key modulator of the UTLS region including the tropopause (Gautam et al., 2009; Lau et al., 2009). Thus, long-term self-calibrated GNSS RO data from various RO missions will help to provide valuable information on the regional climate change in future as indicated by several studies (see, e.g., Schmidt et al., 2008; Steiner et al., 2011, 2013).

The objective of this study is to examine interannual variability of temperature in the UTLS region over the GBM basin using approximately 8 years of monthly accumulated RO data from the COSMIC mission (August 2006- December 2013), together with global reanalysis fields from European Centre for Medium-Range Weather Forecasts reanalysis (ERA-Interim, Dee et al., 2011) and Modern-Era Retrospective Analysis for Research Application (MERRA, Rienecker et al., 2011). Reanalysis products have proven to be very useful in understanding the thermodynamics of the lower atmosphere as well as the tropospheric-stratospheric exchange process by assimilating observations from various platforms including radiosondes, wind profilers, air crafts, and satellites measurements (Poli et al., 2010; Dee et al., 2011; Rienecker et al., 2011). While the primary goal for ERA-Interim has been to address several difficult data assimilation problems in ERA-40 mainly relating to the representation of the hydrological cycle, the quality of the stratospheric circulation, and the consistency in time of reanalysed geophysical fields (Dee et al., 2011), MERRA was developed primarily to improve on various aspects of the hydrologic cycle that were not adequately represented in previous generations of reanalyses (Rienecker et al., 2011). ERA-Interim also assimilates refractivity profiles retrieved from GNSS RO missions from 2001 to reduce temperature biases with respect to radiosondes in the ERA–Interim background (Poli et al., 2010; Dee et al., 2011). Thus, modern reanalysis such as MERRA and ERA-Interim are expected to accurately capture the interannual variabilities of temperature in the UTLS region for the most recent decade.

The remainder of the study is organised as follows. In Section 2, the study region is presented. This is followed in Section 3 by the description of datasets and methods used. The results are presented and discussed in Section 4, and Section 5 concludes the study.

2 Ganges-Brahmaputra-Megha Basin

The GBM river basin in South Asia is a combination of three medium to large river basins, namely, Ganges basin (907,000 km^2), Brahmaputra basin (583,000 km^2) and the Meghna basin (65,000 km^2) (Chowdhury and Ward, 2004). This transboundary river basin with an elevation range from the sea level to more than 8,000 m is shared by 5 countries (India (64%), China (18%), Nepal (9%), Bangladesh (7%) and Bhutan (3%), see, Figure 1). The GBM river basin with a total surface area of approximately 1.75 million km^2 features distinct climatic characteristics owing to its diverse climate and other factors such as high topographic variations, the Indian Monsoon, and its interaction with large scale circulations (e.g., Chowdhury, 2003). For instance, Ganges basin is generally characterised by low precipitation while Brahmaputra and Meghna basins are characterised by high rainfall amount (Mirza et al., 1998). The Himalayan fronts (e.g., Meghalayan Plateau) act as an immediate barrier to the summer monsoonal flow and are usually characterized by pronounced rainfall along the Himalayan fronts and across the southern foothills (Barros et al., 2004).

[FIGURE 1 AROUND HERE.]

The atmospheric conditions over the basin are largely controlled by the monsoonal circulation during summer (e.g., Kripalani et al., 2007), which is often modulated by global and regional large-scale climate variabilities such as ENSO and IOD (e.g., Chowdhury, 2003; Ashok and Saji, 2007). The impact of global warming and regional climate change arising from increasing population and rapid industrial and agricultural activities, and landuse changes across the basin may have resulted in a warmer troposphere over the years (Gautam et al., 2009; Lau et al., 2009).

3 Data and Methods

3.1 FORMOSAT/COSMIC RO Data

COSMIC Level 2 RO data covering the GBM basin (see, Figure 1) for the period April 2006 to December 2013 was obtained from the COSMIC Data Analysis and Archive Center (CDAAC) at the University Corporation for Atmospheric Research (UCAR). CDAAC maintains an archive of RO profiles from many previous and existing RO missions including FORMOSAT/COSMIC (2006-2015), CHAllenging Minisatellite Payload (CHAMP, 2001-2008), Gravity Recovery and Climate Experiment (GRACE, 2006-2015), etc. COSMIC is a six-satellite mission launched on the 14th of April 2006, with the goal of using GNSS RO data for various atmospheric and weather-related applications (Anthes et al., 2008). With an average sounding of around 1,500-2,000 profiles per day (at $\sim$100 m to 1 km vertical resolution and $\sim$300 km horizontal resolution), COSMIC has become a highly successful RO mission with high positive impacts especially on the operational weather forecasts (see e.g., Anthes et al., 2008; Ho et al., 2010; Anthes, 2011) and global atmospheric studies (see e.g., Foelsche et al., 2008; Schmidt et al., 2010). The bending angle (α) with an impact parameter values (a) derived from Doppler shift measurements from RO can be inverted using an Abel transform to recover refractive index (n) profiles (or refractivity, $N = 10^6(n-1)$), which are in fact related to total pressure (P), temperature (T) and water vapour pressure (P_w) as shown in Melbourne et al. (1994). For the dry atmosphere (P_w=0) density profiles are obtained from the known relationship between refractivity and density while pressure and temperature ("dry temperature") can be derived using the hydrostatic equation and equation of state for ideal gas (see, Melbourne et al., 1994). In the presence of water vapour (especially in the lower troposphere), humidity and temperature profiles can be obtained using priori information (or background information) such as numerical weather forecasts. Alternatively, CDAAC also provides a modified refractivity profiles (called "wet profiles") using the one-dimensional Variational (1D-Var) method that combine information provided by GNSS RO and a given priori information in a statistically optimal way (see, http://cdaac-www.cosmic.ucar.edu/cdaac/status.html). The wet and dry profiles mainly differ in the lower troposphere due to presence of water vapour but are highly accurate between 8 and 20 km (see, Anthes et al., 2008). In this study, we used both dry and wet profiles of COSMIC RO to examine their differences over the GBM basin.

The GBM basin recorded 59,419 COSMIC profiles from April 2006 to December 2013, out of which $\sim$14% were found to be of bad quality. Figure 2a shows the temporal record of total monthly profiles recorded during the period, averaging to $\sim$576 profiles in a month from August 2006 to December 2013. The number of profiles drastically went down between late 2010 and 2012 (Figure 2a) due to increasing number of problems in the individual COSMIC satellites (for details, see, http://cdaac-www.cosmic.ucar.edu/cdaac/status.html). Figure 2b shows the distribution of RO data points at various pressure (altitude) levels indicating that COSMIC data is able to penetrate deep into the lower troposphere with more than 56% of the profiles reaching at least 850 hPa ($\sim$1.5 km above MSL). Geographical distribution of COSMIC profiles at 850 hPa ($\sim$1.5 km), 700 hPa ($\sim$3.1 km), 500 hPa ($\sim$6.0 km), and 400 hPa ($\sim$7.5 km) in Figure 3a-d indicates that their locations match very well with the topography of the region (see, Figure 1). A near-complete coverage of the RO data can be seen at 400 hPa ($\sim$7.5 km), which corresponds to the altitude of Himalayas.

[FIGURE 2 AROUND HERE.]

[FIGURE 3 AROUND HERE.]

3.2 Reanalysis Products

The temperature profiles of COSMIC RO data over the GBM region were compared with two high-resolution modern reanalysis products, (a) Modern-Era Retrospective Analysis for Research Application (MERRA, Rienecker et al., 2008) and European Centre for Medium-Range Weather Forecasts (ECMWF) retrospective analysis (ERA-Interim, Dee et al., 2011), both of which were developed to address specific problems in the previous reanalysis systems. MERRA is produced by the state-of-art Goddard Earth Observing System Data Assimilation System, version 5 (GOES-5) general circulation model (GCM) at National Aeronautic and Space Administration (NASA), US. GEOS-5 assimilates data from a wide variety of observing systems (e.g., *in-situ*, satellites, etc.) to produce a consistent set of spatio-temporal meteorological and climatic variables since the beginning of the satellite-era (i.e., 1979). An improved land-process model known as the *Catchment Land Model* has been integrated into the GCM to improve the global hydrological cycle (Rienecker et al., 2008). GEOS-5 is run at a horizontal resolution of $1/2^\circ \times 2/3^\circ$ (or $\sim$50$\times$70 km) and has 72 vertical layers extending from the surface through to the stratosphere. Atmospheric variables (e.g., temperature, humidity) are produced at various temporal scales ranging from 3-hourly at $1.5^\circ \times 1.5^\circ$ (or $\sim$150$\times$150 km) spatial resolution), to monthly scales at the nominal horizontal resolution. GEOS-5 uses radiosondes as the predominant source of information in the model atmosphere, which are further augmented by other atmospheric sensors such as dropsondes, pilot balloons, and raw radiance measurements from satellites (e.g., Advanced MSU) that are weighted according to their observational error variances (see, Rienecker et al., 2008, for details).

ERA-Interim is the latest global atmospheric reanalysis produced by the ECMWF covering the period 1979 to present (Dee et al., 2011). ERA-interim builds on the previous generation of re-

analyses (such as ERA-15 and ERA-40) at the ECMWF with improved model aspects, more advanced assimilation techniques (e.g., 4D Variational Schemes) and better land surface model, and assimilates the latest atmospheric profiles retrieved from the GNSS RO data. The products simulated by ERA-Interim include a large variety of 3-hourly surface parameters, and 6-hourly upper-air parameters from the surface up to 0.1 hPa (stratosphere), which are reported at 60 vertical levels at ∼79x∼79 km spatial resolution (or at spectral resolution of T255). Because ERA-Interim uses newly derived radiosone temperature bias adjustment as well as GNSS RO data, the differences between ERA-Interim and COSMIC RO are likely to be biased. Poli et al. (2010) found that GNSS RO data helps to reduce temperature bias at the tropopause and stratosphere but found drying effect in the mean water-vapour content in the tropics in ERA–Interim. Monthly mean temperature at 14 pressure levels from 500 hPa to 10 hPa were obtained from both MERRA (see, http://disc.sci.gsfc.nasa.gov/daac-bin/FTPSubset.pl) and ERA-Interim (see, http://apps.ecmwf.int/datasets/data/interim-full-daily/levtype=sfc/) to compare their results with those of COSMIC RO data over the GBM basin.

3.3 Ocean-atmospheric indices

We used three ocean-atmospheric indices namely, (a) El Niño Southern Oscillation Index (ENSO), (b) Indian Ocean Dipole (IOD), and (c) quasi-biennial oscillation (QBO) that are commonly associated with significant fluctuations in UTLS temperatures. ENSO is commonly measured by sea surface temperature (SST) anomalies in the equatorial Pacific ocean, typically over (5°N–5°S, 120°–170°W), which is also known as Niño3.4 (see, Trenberth, 1990). ENSO events are said to occur if SST anomalies exceed 4°C for 6 months or more. Warm and cold ENSO phases are referred to as El Niño and La Niña events, respectively, which are represented by anomalous warming of the central and eastern tropical Pacific (warm phase), and vice versa. ENSO events are marked by significant variations in surface and upper-air conditions such as prolonged droughts and heavy rainfall events at the surface and anomalous warming or cooling of the UTLS region. Based on the Niño3.4 index obtained from the National Oceanic and Atmospheric Administration (NOAA, see, http://www.esrl.noaa.gov/psd/data/climateindices/list/), three El Niño events and four La Niño events have occurred between 2006 and 2013.

IOD is measured by difference of SST anomalies between the western (50°E to 70°E and 10°S to 10°N) and eastern (90°E to 110°E and 10°S to 0°S) equatorial Indian ocean, which is also referred to as Dipole Mode Index (DMI). Positive IOD events are identified by cooler than normal water in the tropical eastern Indian Ocean and warmer than normal water in the tropical western Indian Ocean and are associated with a shift of active convection from eastern Indian Ocean to the west leading to potentially higher than normal rainfall over parts of the Indian subcontinent. DMI indices obtained from http://www.jamstec.go.jp/frsgc/research/d1/iod/ indicated four positive IOD events and two negative IOD events during the last 8 years. QBO is stratospheric phenomenon characterized by

an east–west oscillation in stratospheric winds over a period of approximately 28 months (Baldwin et al., 2001). The QBO dominates variability of the equatorial stratosphere and is easily identified as downward propagating easterly (negative) and westerly (negative) wind regimes and commonly measured by an index computed based on zonal winds at 30 hPa or 50 hPa. A full QBO cycle consists of westerly and easterly phase. QBO indices at 30 hPa were download from NOAA and during the period 2006 to 2013, we found three complete QBO cycles.

3.4 Tropopause temperatures and heights

Due to the complex chemical composition and its response to the variability of troposphere and stratosphere, various methods have been used to define the tropopause such as *lapse-rate tropopause* (LRT), *cold point tropopause* (CPT), *dynamical tropopause* (IPV or isentropic potential vorticity), *ozone tropopause* (OT), and *100 hPa pressure level* (see, Holton et al., 1995; Pan et al., 2004). Of these, LRT has been identified as a key indicator of climate change as the height of LRT is sensitive to bulk changes in the thermal structure of the stratosphere and the troposphere (e.g., Santer et al., 2003a; Sausen and Santer, 2003). Here, we used the LRT (simply referred as tropopause henceforth) based on definition outlined by the WMO (1957): "the lowest level at which the lapse rate decreases to 2ºC/km or less, provided also the average lapse rate between this level and all higher levels within 2 km does not exceed 2°C/km." COSMIC RO data obtained from CDAAC already contain the derived tropopause parameters (heights and temperatures), while MERRA also provides tropopause temperatures and pressures based on the WMO (1957) definition. We did not use ERA-Interim here because we believe that assimilation of GNSS RO data could likely cause bias in trend estimates and variabilities, which will be reported later. The tropopause heights, h_{LRT} (in km) for MERRA was approximated from the tropopause pressures, P (in Pa) using the following relationship (PSAS, 2004):

$$h_{LRT} \equiv 44330.8 - 4946.54 \times P^{0.1902632}. \quad (1)$$

3.5 Principal Component Analysis (PCA)

Monthly accumulated COSMIC RO data were interpolated to a spatial resolution of $0.5^\circ \times 0.5^\circ$ over 14 standard pressure levels from 500-10 hPa (or 7.5-31 km) using the ordinary kriging method (see details in the Supplementary Material). The geostatistical kriging methods have been shown to be more robust and spatially more reliable than other existing methods such as inverse-distance-weighting, Thiessen Polygons (see, e.g., Goovaerts, 2000; Zhang and Srinivasan, 2009). To study the interannual variations of temperature at various pressure levels, monthly temperature at each grid cell were deseasonalized by removing the time mean from each month. We also applied Principal Component Analysis/Empirical Orthogonal Functions (PCA/EOF, Lorenz, 1956; Preisendorfer, 1988) to the deseasonalized tropopause heights and temperatures to extract multiple variability modes associated with various atmospheric-oceanic mechanisms. PCA (hereinafter) is one of the widely used

data exploratory tools used in atmospheric/oceanic science that allows for a space-time display of spatio-temporal data such as temperature in here, in a very few modes. PCA is multipurpose and have been used to study the impact of ENSO and QBO modes at various levels of the atmosphere including the tropopause (see, Randel et al., 2000; Gettelman et al., 2001). The central idea of PCA is to find a set of orthogonal spatial patterns (or EOFs) along with a set of associated uncorrelated time-series or principal components (PCs) that captures most of the observed variance (expressed in %) from the available spatio-temporal data (e.g., temperature). In summary, the EOF decomposition can be written as $\mathbf{X_{(t,s)}} = \mathbf{P_{(t,n)}}\mathbf{E^{T}_{(s,n)}}$ where $\mathbf{X_{(t,s)}}$ is the space (s)-time (t) data with its time-mean or annual cycle removed, $\mathbf{E_{(s,n)}}$ contains the EOFs with n number of retained modes, and $\mathbf{P_{(t,n)}}$ are the PCs obtained by projecting the original data ($\mathbf{X_{(t,s)}}$) on the orthogonal base-functions $\mathbf{E_{(s,n)}}$, i.e., $\mathbf{P_{(t,n)}} = \mathbf{X_{(t,s)}}\mathbf{E_{(s,n)}}$. This method can be applied at various stages of the data in order to find any meaningful links to various dynamics of the climate system using a subset of PCs.

4 Results and Discussion

4.1 Seasonal and interannual variability of UTLS temperature

First, we compared COSMIC profiles (both dry and wet profiles) with temperature and refractivity profiles from 24 radiosonde stations across the GBM basin from August 2006 to December 2013 with 18 of them located within the Indian territory. While the results (see, supplementary material) confirmed those of the previous studies (e.g., Sun et al., 2010; Kumar et al., 2011; Ansari et al., 2015) with anomalously warm bias (up to 4°C) for those old radiosondes (also known as IMD-MK4) over India, results from recently upgraded three radiosondes (over India) also showed reduced but substantial warm bias (up to 2.7°C) with very high standard deviations in the UTLS region (see supplementary material). This suggests that newly installed GPS-based sondes still did not achieve the standard that is shown by other radiosonde types despite their recent acceptance in the global weather assimilation systems (see, Kumar et al., 2011). This further highlights the importance of using RO data in both global assimilation systems and climate variability studies to improve our understanding of upper atmospheric conditions and weather forecasts over the region.

Figure 4 shows the regional mean temporal evolution of UTLS temperature with each time series plotted as anomalies (time mean removed). The temperature anomalies range between ±6°C and shows largest anomalies above 50 hPa (in the lower stratosphere) and below 200 hPa (in the upper troposphere). A strong seasonal cycle is evident in the lower troposphere (below 200 hPa) and the stratosphere (above 70 hPa) whereas the seasonal cycle is found to diminish at the tropopause region (150-70 hPa) in some years (2008/2009, 2011/2012). The three datasets (COSMIC, MERRA, and ERA-Interim) agree very well above 200 hPa where water vapour is negligible. Below 200 hPa, however, COSMIC "dry" profiles (Figure 4a) show anomalously cold bias compared to the reanalysis products (Figure 4b-c), where priori information (background data) is required to retrieve humid-

ity and temperature profiles. The relative difference between COSMIC RO and reanalysis products were found to be very similar with 1.23°C and 1.22°C for MERRA and ERA-Interim, respectively between 200 hPa and 70 hPa while the differences between MERRA and ERA-Interim was ±0.5°C. The annual cycle of temperature was plotted for four pressure levels: (a) 200 hPa, (b) 100 hPa, (c) 70 hPa, and (d) 50 hPa in Figure 5 to estimate absolute bias in reanalysis products. The seasonality of temperature was captured very well at all pressure levels with MERRA and ERA-Interim showing warm bias at all pressure levels. Both the reanalysis products showed warm bias during monsoon period (by ~ 1°C) in the troposphere (200 hPa, Figure 5a), consistent warm bias at 100 hPa (often used as proxy for tropical tropopause, Figure 5b), and by up to 2°C at 70 hPa (Figure 5c). The two reanalysis products showed quantitatively similar patterns except at 100 hPa where ERA-Interim showed smaller bias with COSMIC RO during the monsoon period, probably due to assimilation of GNSS RO data.

[FIGURE 4 AROUND HERE.]

[FIGURE 5 AROUND HERE.]

Interannual variations were also captured during the last 8 years with relatively lower temperature in the troposphere in 2009/2010 winter and early 2013, and low stratospheric temperature during 2007/2008, 2008/2009, and 2012/2013 winters. These variations are clearly shown by removing their mean annual cycle as shown in Figure 6 where warm (2006/2007, 2009/2010, and 2010/2011) and cold (2007/2008, 2008/2009, 2011/2012, and 2012/2013) temperatures were recorded at various levels in the stratosphere. A very warm (up to 1.5°C) temperature was also recorded at the tropopause level in 2006/2007, 2009/2010, and 2012/2013. These warm/cold anomalies are mainly driven by various atmospheric/oceanic phenomenon that affect the global climate including the troposphere and stratosphere e.g., ENSO, QBO, and possibly local SST anomalies. The warm anomalies at the tropopause level during 2006/2007, 2009/2010, and 2012/2013 coincides with warm (El Niñ) ENSO phase, while anomalously warm temperatures during 2009/2010 and 2010/2011 coincides with the stratospheric sudden warming (SSW) events. SSW are stratospheric events where polar vortex of westerly winds in the winter polar region (Northern Hemisphere) slows down or even reverses direction over the course of a few days, which are accompanied by sudden rise in stratospheric temperature by several tens of °C (e.g., Hansen et al., 2014). These anomalously warm temperatures in the upper stratosphere (above 30 hPa) were associated with very cold temperature anomalies between the tropopause and 50 hPa with a decrease of about 5°C from its temporal mean during the 2008/2009 strong SSW event. The results are consistent with those from (Resmi et al., 2013), who used ERA-Interim and observations from six radiosonde stations across India. Their study also found that surface temperatures react strongly to these major SSW events. All the three datasets showed quantitatively similar interannual variations at all pressure levels from 500 hPa to 10 hPa indicating that both MERRA and ERA-Interim products were of considerably high quality despite

their low vertical resolution. This consistency has also been already noted in ERA-Interim by Poli et al. (2008, 2010) on a global scale. The stratosphere responds to major global climatic events such as Brewer-Dobson circulation, solar radiations, and natural and man-made aerosol forcings (e.g., Fueglistaler et al., 2009), and have been found to influence global weather conditions in the lower troposphere (e.g., Foelsche et al., 2008; Seidel et al., 2011) including persistent occurrence of thin cirrus clouds over the Indian subcontinent (see, Sridharan et al., 2011).

[FIGURE 6 AROUND HERE.]

We also plotted temperature anomalies at (a) 200 hPa, (b) 100 hPa, (c) 70 hPa, and (d) 50 hPa in Figure 7a-d together with ocean-atmospheric indices in Figure 7e. The 200 hPa temperature anomalies clearly shows the influence of 2009/2010 El Niño event (Figure 7a) with a decrease of $\sim$1.5°C in January 2010. The 2009/2010 El Niño event commenced in May 2009, reaching its peak in late December 2009 before slowing down in the first quarter of 2010. The tropospheric (200 hPa) temperatures are negatively correlated with 100 hPa, which is visible especially during the major ENSO events of 2009/2010 (Figure 7b). The 100 hPa level, which is often used as proxy for tropopause, also shows some pattern of QBO in 2008/2009 and 2010/2011. However, it indicated warm temperature in 2013 despite continuing periods of negative QBO. The temperature anomalies at 70 hPa and 50 hPa (Figure 7c-d) primarily indicates the temporal structure of major SSW events that were observed in Figure 6. One major SSW event (in 2009/2010) and two major SSW events (2010/2011) have occurred during the last 8 years, which is clearly seen at 50 hPa (lower stratospheric layer considered to be very close to the onset of QBO). The stratospheric temperature anomalies at 70 hPa and 50 hPa also shows a decrease of temperature by about 1°C in 2007, which did not correspond well with any of the indices. Correlation coefficients between temperatures at these four pressure levels and atmospheric/ocean indices given in Table 1 indicates that ENSO dominates its influence in the UTLS region showing maximum influence in the tropopause region with a correlation of 0.82 (for lag of 1 month). Warmer (colder) SST leads to stronger (weaker) convection resulting in colder (warmer) tropopause temperatures and are negatively correlated with tropospheric temperatures. The correlation results were reported only for COSMIC RO as both MERRA and ERA-Interim were found to be highly skillful in depicting the interannual variability (see, Table 1).

[FIGURE 7 AROUND HERE.]

It is worth mentioning that IOD mode was found to be significantly correlated (at 95% confidence interval) to the ENSO mode during the period 2006 to 2013 with a correlation coefficient of 0.42. Nevertheless, the relationship between IOD and temperature is significant only in the troposphere where convection is maximum. For example, correlation between IOD and 200 hPa was -0.42 (see Table 1) whereas it increased to -0.53 at 400 hPa. Temperature at 100 hPa (or the proxy tropopause) level generally provides a good approximation of the QBO signal (e.g., Reid and Gage, 1985; Randel

et al., 2000; Liang et al., 2011) such that its correlation was reported as high as 0.86 over the equatorial region from 2004 to 2010 (see, Liang et al., 2011). However, the relationship between QBO and temperature at 100 hPa was was found to be negative and substantially low, which could be due to prolonged westerly phases from June 2008-January 2010 followed by a step easterly phase peaking in June 2010. The correlation between QBO and 100 hPa temperature was 0.47 and reaches to 0.53 at 50 hPa, both of which are still statistically significant at 95% confidence interval. The relationship between QBO and Niño3.4 diminished after mid-June 2009 implying that its influence over troposphere upwelling in the Indian monsoon region (see e.g., Chattopadhyay and Bhatla, 2002; Resmi et al., 2013; Liang et al., 2011) may have also altered due to stronger easterly phases and prolonged westerly phases.

Trends in temperature were calculated from the deseasonalized temperature anomalies using the non-parametric Sen's slope estimator (Sen, 1968) and their significance were tested at 95% confidence level using the Mann-Kendall's non-parametric test (Mann, 1945; Kendall, 1962). The linear trends estimated from four pressure levels shown in Figure 7 is given in Table 2. Based on Figures 7a-d, we found a slight increase in temperature (0.02 ± 0.02 based on COSMIC RO) in the upper troposphere (at 200 hPa level), although not significant, and decrease in temperature (-0.04 ± 0.05°C based on COSMIC RO) at the tropopause level (indicated by the 100 hPa level). We found a pronounced cooling (-0.07 ± 0.05°C based on COSMIC RO) at 70 hPa level compared to 50 hPa level (-0.02 ± 0.04°C, also based on COSMIC RO) during the past 8 years. This warming (cooling) of the troposphere (stratosphere) has been well simulated by the global climate models (GCMs) and is believed to be in response to the increasing concentrations of greenhouse gases (e.g., Santer et al., 2005; IPCC, 2007; Santer et al., 2008; IPCC, 2013; Lott et al., 2013). These trends were also found to be very consistent in the two reanalysis products (MERRA and ERA-Interim) except at 100 hPa level where MERRA data did not show any trend (see, Table 2). The uncertainties in trend estimates were relatively larger than the trend themselves due to the short time-span but nevertheless the trends are clearly visible at different levels (see Figure 7).

4.2 Trends and variability of tropopause heights and temperatures

While it is possible to derive interannual variability of the tropopause based on the 100 hPa level, Seidel et al. (2001) reported that it is a poor surrogate of tropical tropopause due to significantly lesser spatial and temporal variability than the heights of the LRT and CPT. In particular, their study also showed that 100 hPa level resides in the stratosphere during the northern hemisphere (NH) summer and in the troposphere during the NH winter, thus, indicating warmer temperatures than LRT and CPT. In this section, we applied PCA to examine the variability of tropopause (i.e., LRT tropopause) parameters (temperatures and heights) from COSMIC RO and MERRA over the GBM basin. The spatial domain shown in Figure 1 falls within the tropics and the subtropics where the tropopause height (temperature) is considered to be around 16 km ($\sim$-82°C close to the equator)

(e.g., Reid and Gage, 1985; Randel et al., 2000; Seidel et al., 2001). The annual mean and standard deviation of tropopause temperatures and heights over the region are plotted in Figures 8 and 9 to show the spatial variability of the tropopause. The tropopause is generally colder (higher) in south (closer to the equator) reaching a minimum (maximum) of -81.5°C (16.9 km) over southern Myannmar (Figures 8a and 9a). While the temperature gradually increases from south to north (from -81.5°C to -69.5°C, based on COSMIC RO in Figure 8a), its heights are more or less homogenous at around 16.8 km below 29°N with its boundary roughly falling on the northern boundaries of Bhutan. However, its height changes steeply by around 2 km from 29°N to 35°N, which also indicated the highest standard deviation ($\sim$1.8 km, Figure 9b). In this region, the standard deviations of up to 6°C were recorded in COSMIC RO data (Figure 8b).

[FIGURE 8 AROUND HERE.]

[FIGURE 9 AROUND HERE.]

The tropopause over the GBM basin often reaches as high as 18 km in response to the Indian summer monsoon when intense convective activities occur and as low as 10 km in winter due to weak convection. The spatial patterns of tropopause shown by MERRA were consistent with COSMIC RO but were found to be more zonally homogenous, warmer (by up to 4°C in the north) and lower (by $\sim$1 km) over the region. This warm bias was also observed in ERA-Interim at 100 hPa (see Figure 5b) but was lower than MERRA especially during the monsoon. The impact of warm (and lower) tropopause in the relanalysis over the region could perhaps lead to underestimation of monsoon rainfall as higher tropopause indicate deeper convection and thus, more rainfall. The annual cycle of tropopause temperatures and heights of COSMIC RO and MERRA are shown in Figure 10. The area-averaged temperatures (heights) of COSMIC RO reaches minimum (maximum) in June while MERRA shows large (but consistent) warm bias (1.0-2.5°C) and significantly lower height (by up to 1.2 km from May to December). MERRA also shows tropopause temperature minimum in July instead of June (Figure 10a). The bias in tropopause height may partly related to our approximation based on Eq. 1 but it should be noted that errors in tropopause heights cause large errors in its temperature due to the lapse-rate criterion. The warm bias in observed in reanalysis products were thought to mainly stem from assimilation of large observations from aircrafts and satellites (see e.g., Dee et al., 2011, and references therein). The uncertainties in temperature and height indicated by error bars in Figure 10 shows that there are large variations in tropopause (temperatures and heights) especially during winter and spring and could be related to dirunal variations (Mehta et al., 2010).

[FIGURE 10 AROUND HERE.]

The annual cycle was removed from each grid cells to examine the interannual variability of tropopause parameters and linear trends were also calculated based on area-averaged time series

anomalies over the period August 2006 to December 2013. The linear trend estimates and their uncertainties are given in Table 3. In general, tropopause appears to be cooling (increasing) at rate of -0.039 ± 0.05°C (6.01 ± 5.02 meters) during the period (see Table 3), which is to some degree reflected in the MERRA product. However, MERRA shows negligible cooling compared to COSMIC RO whereas its height increase is exaggerated and are not consistent with the temperature decrease. The increasing (decreasing) tropopause heights (temperatures) has been consistently observed in GNSS RO retrieved parameters over the years at both global and regional scale (e.g., Schmidt et al., 2008, 2010; Khandu et al., 2011), which is evidently in response to ehnanced warming in the upper troposphere and substantial cooling in the lower stratosphere.

To study the influence of global ocean-atmospheric phenomenon such as ENSO, QBO, and IOD on the interannual variation of tropopause heights and temperatures, we applied PCA to the detrended temperature (and height) time-series anomalies to extract multiple leading modes of variability. PCA is particularly relevant here because tropopause is a transitional layer that responds to perturbations from both the troposphere and stratosphere, which makes it difficult to understand their variability modes. Figure 11 shows the EOFs (or spatial maps) for the first three leading modes of variability. The first EOF accounts for variability of $\sim$73% (COSMIC RO) and 63$\sim$% (MERRA) indicating positive anomalies (up to 1.1°C) across the GBM basin. The spatial patterns of EOF 1 appears rather symmetric about 29°N in COSMIC RO but seems to be shifted slightly southwards in MERRA (Figures 11a and 11d). Their corresponding PCs shown in Figure 12a were found to be highly correlated with Niño3.4 index at 0.77 (COSMIC RO) and 0.78 (MERRA) with a lag of one month. Thus, the impact of ENSO is found to be maximum over the Himalayan region. We also found statistically significant correlation between PC 1 and IOD with a correlation of 0.35 for both COSMIC RO and MERRA (with a lag of 2 months) indicating that positive IOD events induces cooler tropopause. The correlation coefficients are provided in Table 4.

[FIGURE 11 AROUND HERE.]

[FIGURE 12 AROUND HERE.]

The second EOF (Figures 11b and 11e) shows a diagonal (dipole) pattern with positive (negative) anomalies in the northwest (southeast) and accounts for $\sim$10% (COSMIC) and $\sim$18% (MERRA) of variability. Their corresponding PCs were found to be correlated with the QBO index at 0.40 (COSMIC RO) and 0.53 (MERRA) (at zero lag). It is not surprising that the relationship between PC 2 and QBO is rather low compared to the equatorial (or tropical) tropopause since the impact of QBO is maximum around the equator (between $\pm 15°$). However, it is interesting to find that its impacts are diagonal over the region (from 2006-2013), which usually is symmetric around the equator (e.g., Reid and Gage, 1985; Randel et al., 2000; Gettelman et al., 2001). QBO is a well-known interannual signal observed in the tropical tropopause parameters such as tropopause responds to stratospheric variations to maintain the thermal wind balance. Liang et al. (2011) found a correlation of 0.86

between QBO and temperature anomalies (at 100 hPa level) in the equatorial region. The third EOF (Figure 11c and 11f) explains about 5% (COSMIC RO) and 10% (MERRA) of the variability and shows positive (negative) anomalies below (above) 30°N, although MERRA shows a diagonal dipole pattern similar to EOF 2. Their corresponding PCs were found to be moderately correlated with ENSO and IOD but not QBO.

The tropopause heights are negatively correlated with their temperatures and therefore, should vary inversely with its temperature, i.e., increase in tropopause height with drop in temperature. The first three leading EOFs are shown in Figure 13 and their corresponding PCs are plotted in Figure 14. While tropopause temperature shows maximum variation along 29°N, tropopause height shows largest anomalies above 25°N (Figures 13a and 13d) in response to ENSO events indicating that its impacts are felt mostly in the subtropics. The correlation (see, Table 4) between PC 1 and Niño3.4 index was -0.74 (COSMIC RO) and -0.75 (MERRA). IOD also shows a modest relationship with a correlation of around 0.37 for both the datasets. The QBO structures over the region is rather complicated and difficult to explain but nevertheless follows its temperature pattern as shown in Figures 11b and 11d. The correlation between PC 2 and QBO index was higher for MERRA (0.53 at zero lag) compared to COSMIC RO, which did not capture the QBO signals very well. Nevertheless, it shows a modest correlation (0.36 at zero lag). We also computed trends based on the extracted ENSO and QBO modes but no significant trends were detected in tropopause temperatures and heights. Thus, decreasing (increasing) tropopause temperatures (heights) may be related to tropospheric warming (as evidenced by enhanced cooling at 200 hPa level) that could be induced by increasing concentrations of greenhouse gases. Since ENSO and IOD are somewhat related (see, also Ashok and Saji, 2007), it is difficult to separate the two modes in tropopause parameters but it should be noted that ENSO events dominate the tropopause variability in the region with maximum impacts in the subtropical region.

[FIGURE 13 AROUND HERE.]

[FIGURE 14 AROUND HERE.]

To show the influence of ENSO mode on the tropopause, we have plotted the seasonal mean time-series anomalies of tropopause temperatures and heights in Figure 15. Seasonal mean anomalies were obtained by multiplying EOF 1 and PC 1. Figure 15 indicates that ENSO influences the tropopause during the winter (e.g., 2009-2010, 2012-2013) (when ENSO was at its peak). Nevertheless, it should be mentioned that maximum impact was also felt during autumn (in 2007 and 2011) and spring (in 2008) during both El Niño and La Niña periods. The largest anomaly was found in 2009/2010 winter where tropopause temperature (height) increased (decreased) by about 1.5°C (300 meters) due to a major El Niño event. La Niña periods (e.g., 2007/2008, 2010/2011) are mainly associated with above normal rainfall in the GBM basin, which is also associated with deep convections in the troposphere (see Figure 15). This deep convections are associated with colder and higher

tropopause. QBO and SSW events are also closely related such that it also induces large tropopause perturbations, which is especially evident in PC 2 (Figures 12b and 14b) where tropopause showed maximum amplitude in 2008/2009 early spring.

[FIGURE 15 AROUND HERE.]

5 Conclusions

Several GNSS RO missions were launched in the past decade delivering thousands of high-quality, global observations of the Earth's atmosphere (ionosphere, stratosphere, and troposphere) for various weather and climate applications. This study examined the interannual variability of temperature in the UTLS region including tropopause temperatures and heights over the GBM basin in South Asia based on 89 months (August 2006 to December 2013) of COSMIC RO data and two global reanalysis products (MERRA and ERA-Interim). The GBM basin received a total of 59,419 RO profiles from six COSMIC satellites between April 2006 and December 2013, with an average of $\sim$576 well-distributed profiles/month from August 2006 to December 2013. More than 56% of the profiles reached at least 1.5 km above the mean sea level height. While there are substantial absolute warm bias (by up to 2°C at 200-50 hPa level) in MERRA and ERA-Interim in the UTLS region, they were found to be consistent over time resulting in a relative bias of $\pm$0.5°C. This enabled accurate representation of interannual variability of the UTLS temperature despite low vertical resolution. In the upper troposphere (at 200 hPa level), COSMIC RO data (dry profiles) showed a cold bias of around 1°C in the peak monsoon period. The UTLS temperature showed considerable interannual variability in the past 8 years (2006-2013) as well as modest changes in tropospheric and stratospheric temperatures. The cold (warm) anomalies in the upper troposphere indicated by 200 hPa level (tropopause region indicated by 100 hPa level) coincides with the warm ENSO phase (El Niño events) while SSW signals were seen in the stratospheric temperature anomalies. In particular, temperature at 200 hPa reduced by $\sim$1.5°C during the last major El Niño event of 2009/2010. The SSW signatures were captured best at 50 hPa level, which was marked by one major SSW event (2008/2009 winter) and two minor SSW events in 2010/2011 leading to decrease in temperature at the tropopause region. ENSO has the maximum influence around the tropopause region (indicated by 100 hPa level) with a correlation of 0.82 (at 1 month lag) while QBO showed maximum influence at the 50 hPa level (with a correlation of 0.53).

The relationship between ENSO and QBO was reported to be considerably high between 2004 and 2008 (see, Liang et al., 2011) but has since diminished by mid-2008 due to a persistent westerly phase that lasted for 21 months from June 2008 to January 2010. Thus, the combined impacts of ENSO and QBO are not well understood. For IOD, although considered to be relatively mild compared to ENSO, there exists significant correlation between Dipole Ocean Index (DMI) and temperature at 200 hPa level (with a correlation of -0.42) indicating that IOD impacts are felt mostly

in the troposphere. In general, we found an upper tropospheric warming and lower stratospheric cooling with highest warming (cooling) at 200 hPa level (70 hPa level). These trends are consistent with existing global warming trends and has been documented previously by many studies (see, e.g., IPCC, 2007, 2013, and references therein). The trends and temporal variations were well captured by both MERRA and ERA-Interim. It should be noted however that, trends are more pronounced in the UTLS region than in the lower tropospheric or the surface (Randel et al., 2000; Gettelman et al., 2001; Seidel et al., 2011).

The tropopause temperatures and heights derived from COSMIC RO and MERRA were investigated in detail due to there perceived importance in climate detection and attribution studies (see, e.g., Santer et al., 2003a, 2008; IPCC, 2007). The tropopause temperatures gradually increased from south to north (from -81.5°C to -69.5°C), while the tropopause heights were found to more or less homogenous over the region (at 16.8 km), although a step decline in heights was observed above 29°N. It should be noted however, that both tropopause temperature and height indicated significant seasonal variability with its heights reaching as high as 18.5 km during the peak monsoon period. The temperatures and heights, as mentioned were found to be warmer (by up to 4°C) and lower (by 1 km) in MERRA and ERA-Interim products. Trends in tropopause temperatures and heights were consistent with the overall UTLS temperature (especially the 100 hPa level) trends indicating a decrease (increase) in temperatures (heights). These trends indicate that tropopause is sensitive to global change and is detectable even on a shorter time period. One potential impact due to increasing tropopause height is increase in water vapour in the lower stratosphere as it allows larger saturation mixing ratios to enter the stratosphere.

Using PCA, we extracted the interannual variability modes of the regional tropopause temperatures and heights. The results showed continued dominance of ENSO (see e.g., Reid and Gage, 1985; Randel et al., 2000; Gettelman et al., 2001; Seidel and Randel, 2006; Liang et al., 2011) with anomalies of up to 1.1°C in the subtropics. ENSO explains about 73% (COSMIC RO) and 63% (MERRA) of the interannual variability, which is preceded by the QBO mode accounting for $\sim$10% (COSMIC RO) and $\sim$18% (MERRA) of the interannual variability. Their corresponding PCs, particularly PC 1 shows an accurate representation of the ENSO mode (represented by the Niño3.4 index) with a correlation of 0.77 (COSMIC RO) and 0.78 (MERRA) while PC 2 was correlated with QBO at 0.36 (COSMIC RO) and 0.53 (MERRA) against tropopause temperatures. Similar correlation values were found between tropopause heights and ENSO/QBO modes but it should be noted that tropopause heights are inversely correlated with ENSO due to its inverse relation with temperature. ENSO impacts tropopause temperatures and heights mainly during the winter (e.g., 2009-2010, 2012-2013) (when ENSO is at its peak). The largest anomaly was found in 2009/2010 winter when tropopause temperatures (heights) increased (decreased) by about 1.5°C (300 meters) corresponding to a major El Niño event. The IOD mode, on the other hand was moderately related to ENSO and hence were more related to PC 1. A positive IOD is event usually associated with the shift in active

convection from eastern Indian ocean to western Indian ocean, leading to higher than normal rainfall over parts of the Indian subcontinent and East Africa while severe droughts affect the Indonesian region. Thus, positive IOD events should be normally associated with cooler (higher) tropopause temperatures (heights).

Acknowledgement

The first author is deeply grateful to Curtin Strategic International Research Scholarship, Curtin University (Australia) for funding his PhD studies. He is further grateful to Intergovernmental Panel of Climate Change (IPCC) for the scholarship. J. Awange appreciates the financial support from both Alexander von Humboldt and Japan Society of Promotion of Science for his stay at Karlsruhe Institute of Technology (Germany) and Kyoto University (Japan), respectively. Forootan is grateful for the research grant from the German Aerospace Center (DLR). The authors are highly grateful to the COSMIC Data Analysis and Archival Center (CDAAC, http://cdaac-www.cosmic.ucar.edu/cdaac/) for providing both COSMIC radio occultation profiles, regional radiosonde datasets, and re-analysis profiles used in this study. The authors are also thankful to the MERRA for providing high-resolution global atmospheric products for regional studies. This is a TiGeR publication number (XXX).

References

Ansari, M. I., Madan, R., and Bhaita, S.: Verification of quality of GPS based radiosonde data, Mausam, 66, 367–374, available at: metnet.imd.gov.in/mausamdocs/16632_F.pdf, 2015.

Anthes, R. A.: Exploring Earth's atmosphere with radio occultation: contributions to weather, climate and space weather, Atmos. Meas. Tech., 4, 1077—1103, doi:10.5194/amt-4-1077-2011, 2011.

Anthes, R. A., Ector, D., Hunt, D. C., Kuo, Y. H., Rocken, C., Schreiner, W. S., Sokolovskiy, S. V., Syndergaard, S., Wee, T. K., Zeng, Z., Bernhardt, P. A., Dymond, K. F., Chen, Y., Liu, H., Manning, K., Randel, W. J., Trenberth, K. E., Cucurull, L., Healy, S. B., Ho, S. P., McCormick, C., Meehan, T. K., Thompson, D. C., and Yen, N. L.: The COSMIC/FORMOSAT-3 Mission: Early Results, Bull. Amer. Meteor. Soc., 89, 313—-333, doi:10.1175/BAMS-89-3-313, 2008.

Ashok, K. and Saji, N. H.: On the impacts of ENSO and Indian Ocean dipole events on sub-regional Indian summer monsoon rainfall, Natural Hazards, 42, 273–285, doi:10.1007/s11069-006-9091-0, 2007.

Awange, J. L.: GNSS Remote Sensing of the Environment, in: Environmental Monitoring using GNSS: Global Navigation Satellite Systems, p. 382, Springer Berlin Heidelberg, 2012.

Baldwin, M. P., Gray, L. J., Dunkerton, T. J., Hamilton, K., Haynes, P. H., Randel, W. J., Holton, J. R., Alexander, M. J., Hirota, I., Horinouchi, T., Jones, D. B. A., Kinnersley, J. S., Marquardt, C., Sato, K., and Takahashi, M.: The quasi-biennial oscillation, Reviews of Geophysics, 39, 179—229, doi:10.1029/1999RG000073, 2001.

Barros, A. P., Kim, G., Williams, E., and Nesbitt, S. W.: Probing orographic controls in the Himalayas during the monsoon using satellite imagery, Nat. Hazards Earth Syst. Sci., 4, 29–51, doi:10.5194/nhess-4-29-2004, 2004.

Bindoff, N. L., Stott, P. A., AchutaRao, K. M., Allen, M. R., Gillett, N., Gutzler, D., Hansingo, K., Hegerl, G., Hu, Y., Jain, S., Mokhov, I. I., Overland, J., Perlwitz, J., Sebbari, R., and Zhang, X.: Detection and Attribution of Climate Change, in: Climate Change 2013: The Physical Science Basis. Contribution of Working Group I to the Fifth Assessment Report of the Intergovernmental Panel on Climate Change, edited by Stocker, T. F., Qin, D., Plattner, G.-K., Tignor, M., Allen, S., Boschung, J., Nauels, A., Xia, Y., Bex, V., and Midgley, P., Cambridge University Press, Cambridge, United Kingdom and New York, NY, USA, 2013.

Chattopadhyay, J. and Bhatla, R.: Possible influence of QBO on teleconnections relating Indian summer monsoon rainfall and sea-surface temperature anomalies across the equatorial pacific, International Journal of Climatology, 22, 121–127, doi:10.1029/2010JD014841, 2002.

Chowdary, J. S., John, N., and Gnanaseelan, C.: Interannual variability of surface air-temperature over India: impact of ENSO and Indian Ocean Sea surface temperature, International Journal of Climatology, 34, 416–429, doi:10.1002/joc.3695, 2014.

Chowdhury, M. D. R. and Ward, N.: Hydro-meteorological variability in the greater Ganges–Brahmaputra–Meghna basins, International Journal of Climatology, 24, 1495–1508, doi:10.1002/joc.1076, 2004.

Chowdhury, M. R.: The El Niño-Southern Oscillation (ENSO) and seasonal flooding – Bangladesh, Theoretical and Applied Climatology, 76, 105–124, doi:10.1007/s00704-003-0001-z, 2003.

Cucurull, L., Derber, J. C., Treadon, R., and Purser, R.: Assimilation of Global Positioning System radio occultation observations into NCEP's Global Data Assimilation System, Mon. Weather Rev., 35, 3174–3193, doi:10.1175/MWR3461.1, 2007.

Das Gupta, M., Das, S., Prasanthi, K., and Pradhan, P. K.: Validation of upper-air observations taken during the ARMEX-I and its impact on the global analysis-forecast system, MAUSAM, 56, 139–146, 2005.

Dee, D. P., Uppala, S. M., Simmons, A. J., Berrisford, P., Poli, P., Kobayashi, S., Andrae, U., Balmaseda, M. A., , Balsamo, G., Bauer, P., Bechtold, P., Beljaars, A. C. M., van de Berg, L., Bidlot, J., Bormann, N., Delsol, C., Dragani, R., Fuentes, M., Geer, A. J., Haimbergere, L., Healy, S. B., Hersbach, H., Holm, E. V., Isaksen, L., Kållberg, P., Köhler, M., Matricardi, M., McNally, A. P., Monge-Sanz, B. M., Morcrette, J.-J., Park, B.-K., Peubey, C., de Rosnay, P., Tavolato, C., Thépaut, J.-N., and Vitarta, F.: The ERA-Interim reanalysis: Configuration and performance of the data assimilation system, Quarterly Journal of the Royal Meteorological Society, 137, 553—597, doi:10.1002/qj.828, 2011.

Foelsche, U., Borsche, M., Steiner, A. K., Gobiet, A., Pirscher, B., Kirchengast, G., Wickert, J., and Schmidt, T.: Observing upper troposphere–lower stratosphere climate with radio occultation data from the CHAMP satellite, Climate Dynamics, 31, 49–65, doi:10.1007/s00382-007-0337-7, 2008.

Fueglistaler, S., Dessler, A. E., Dunkerton, T. J., Folkins, I., Fu, Q., and Mote, P. W.: Tropical tropopause layer, Rev. Geophys, 47, doi:10.1029/2008RG000267, 2009.

Gautam, R., Hsu, N. C., Lau, K. M., Tsay, S. C., and Kafatos, M.: Enhanced Pre-Monsoon Warming over the Himalayan-Gangetic Region from 1979 to 2007, Geophysical Research Letters, 36, doi:10.1029/2009GL037641, 2009.

Gettelman, A. and de F. Foster, P.: A Climatology of the Tropical Tropopause Layer, Journal of the Meteorological Society of Japan, 80, 911–924, doi:10.1029/2006JD007363, 2002.

Gettelman, A., Randel, W. J., Massie, S., Wu, F., Read, W. G., and Russell, J. M.: El Ni no as a Natural Experiment for Studying the Tropical Tropopause Region, J. Climate, 14, 3375–339, doi:10.1175/1520-0442(2001)014<3375:ENOAAN>2.0.CO;2, 2001.

Goovaerts, P.: Geostatistical approaches for incorporating elevation into the spatial interpolation of rainfall, Journal of Hydrology, 228, 113–129, doi:10.1016/S0022-1694(00)00144-X, 2000.

Hansen, F., Matthes, K., Petrick, C., , and Wang, W.: The influence of natural and anthropogenic factors on major stratospheric sudden warmings, Journal of Geophysical Research, 119, 8117–8136, doi:10.1002/2013JD021397, 2014.

Healy, S. B. and Thépaut, J.-N.: Assimilation experiments with CHAMP GPS radio occultation measurements, Q. J. R. Meteorol. Soc., 132, 605–623., doi:10.1256/qj.04.182, 2006.

Ho, S. P., Zhou, X., Kuo, Y. K., Hunt, D., and Wang, J. H.: Global Evaluation of Radiosonde Water Vapor Systematic Biases using GPS Radio Occultation from COSMIC and ECMWF Analysis, Remote Sens., 2(5), 1320–1330, doi:10.3390/rs2051320, 2010.

Holton, J. R., Haynes, P. H., McIntyre, M. E., Douglass, A. R., Rood, R. B., and Pfister, L.: Stratosphere-troposphere exchange, Review of Geophysics, 35, 403–439, doi:10.1029/95RG02097, 1995.

IPCC: Summary for Policymakers, in: Climate Change 2007: The Physical Science Basis. Contribution of Working Group I to the Fifth Assessment Report of the Intergovernmental Panel on Climate Change, edited

by Solomon, S., Qin, D., Manning, M., Chen, Z., Marquis, M., Averyt, K., M.Tignor, and Miller, H., Cambridge University Press, Cambridge, United Kingdom and New York, USA, 2007.

IPCC: Summary for Policymakers, in: Climate Change 2013: The Physical Science Basis. Contribution of Working Group I to the Fifth Assessment Report of the Intergovernmental Panel on Climate Change, edited by Stocker, T. F., Qin, D., Plattner, G. K., Tignor, M., Allen, S. K., Boschung, J., Nauels, A., Xia, Y., Bex, V., and Midgley, P., Cambridge University Press, Cambridge, United Kingdom and New York, USA, 2013.

Karl, T. R., Hassol, S. J., Miller, C. D., and (eds), W. L. M.: Temperature Trends in the Lower Atmosphere: Steps for Understanding and Reconciling Differences, Tech. rep., U.S. Climate Change Science Program, Washington, DC, 2006.

Kendall, M. G.: Rank correlation methods, Journal of the American Statistical Association, 63, 1379–1389, doi:10.1080/01621459.1968.10480934, 1962.

Khandu, Awange, J. L., Wickert, J., Schmidt, T., Sharifi, M. A., Heck, B., and Fleming, K.: GNSS remote sensing of the Australian tropopause, Climate Change, 105, 597–618, doi:10.1007/s10584-010-9894-6, 2011.

Kripalani, R. H., , Oh, J. H., , Kulkarni, A., , Sabade, S. S., and Chaudhari, H. S.: South Asian summer monsoon precipitation variability: Coupled climate model simulations and projections under IPCC AR4, Theoretical and Applied Climatology, 90, 133–159, doi:10.1007/s00704-006-0282-0, 2007.

Krishnamurti, T. N., Stefanova, L., and Misra, V.: Monsoons, in: Tropical Meteorology: An Introduction, p. 423, Springer Berlin Heidelberg, 2013.

Kulkarni, J. R. and Verma, R. K.: On the spatio-temporal variations of the tropopause height over India and Indian summer monsoon activity, Advances in Atmospheric Sciences, 10, 481–488, doi:10.1007/BF02656973, 1993.

Kumar, G., Madan, R., Saikrishnan, K., Kundu, S. K., and Jain, P. K.: Technical and operational characteristics of GPS sounding system in the upper air network of IMD, Mausam, 62, 403–416, available at: metnet.imd.gov.in/mausamdocs/16632_F.pdf, 2011.

Kursinski, E. R., Hajj, G. A., Schofield, J. T., Linfield, R. P., and Hardy, K. R.: Observing Earth's atmosphere with radio occultation measurements using the Global Positioning System, Journal of Geophysical Research, 102, 23 429—23 465, doi:10.1029/97JD01569, 1997.

Lau, W. K. M., Kim, K. M., Hsu, C. N., and Holben, B. N.: Possible influences of air pollution, dust- and sandstorms on the Indian monsoon, Bulletin - World Meteorological Organization, 58, 22–30, 2009.

Lee, I. T., Matsuo, T., Richmon, A. D., Liu, J. Y., Wang, W., Lin, C. H., Anderson, J. L., and Chen, M. Q.: Assimilation of FORMOSAT-3/COSMIC electron density profiles into a coupled thermosphere/ionosphere model using ensemble Kalman filtering, Journal of Geophysical Research, 117, doi:10.1029/2012JA017700, 2012.

Lewis, H. W.: A robust method for tropopause altitude identification using GPS radio occultation data, Geophysical Research Letters, 36, doi:10.1029/2009GL039231, 2009.

Liang, C. K., Eldering, A., Gettelman, A., Tian, B., Wong, S., Fetzer, E. J., and Liou, K. N.: Record of tropical interannual variability of temperature and water vapor from a combined AIRS-MLS data set, Journal of Geophysical Research, 116, doi:10.1029/2010JD014841, 2011.

Lorenz, E. N.: Empirical Orthogonal Functions and Statistical Weather Prediction, Statistical Forecasting Project Scientific Report No. 1, Air Force Research Laboratories, Office of Aerospace Research, USAF, Bed-

ford, MA, USA, available at: http://eaps4.mit.edu/research/Lorenz/Empirical_Orthogonal_Functions_1956.pdf, 1956.

Lott, F. C., Stott, P. A., Mitchell, D. M., Christidis, N., Gillett, N. P., Haimberger, L., Perlwitz, J., and Thorne, P. W.: Models versus radiosondes in the free atmosphere: A new detection and attribution analysis of temperature, Journal of Geophysical Research, 118, doi:10.1002/jgrd.50255, 2013.

Mann, H. B.: Nonparametric Tests Against Trend, Econometrica, 13, 245–259, 1945.

Mehta, S. K., Ratnam, M. V., and Murthy, B. V. K.: Variability of the tropical tropopause over Indian monsoon region, Journal of Geophysical Research, 115, doi:10.1029/2009JD012655, 2010.

Melbourne, W. G., Davis, E. S., Duncan, C. B., Hajj, G. A., Hardy, K. R., Kursinski, E. R., Meehan, T. K., Young, L. E., and Yunck, T. P.: The application of spaceborne GPS to atmospheric limb sounding and global change monitoring, Tech. Rep. JPL-PUBL-94-18, Jet Propulsion Laboratory, California Institute of Technology, Pasadena, CA, United States, 1994.

Mirza, M. M. Q., Warrick, R., Ericksen, N., and Kenny, G.: Trends and persistence in precipitation in the Ganges, Brahmaputra and Meghna river basins, Hydrological Sciences, 43, doi:10.1080/02626669809492182, 1998.

Pan, L. L., Randel, W. J., Gary, B. L., Mahoney, M. J., and Hintsa, E. J.: Definitions and sharpness of the extratropical tropopause: A trace gas perspective, Review of Geophysics, 109, doi:10.1029/2004JD004982, 2004.

Poli, P., Healy, S. B., Rabier, F., and Pailleux, J.: Preliminary assessment of the scalability of GPS radio occultations impact in numerical weather prediction, Geophysical Research Letters, 35, doi:10.1029/2008GL035873, 2008.

Poli, P., Healy, S. B., and Dee, D. P.: Assimilation of Global Positioning System radio occultation data in the ECMWF ERA–Interim reanalysis, Quarterly Journal of the Royal Meteorological Society, 136, doi:10.1002/qj.722, 2010.

Preisendorfer, R. W.: Principal component analysis in meteorology and oceanography, Elsevier, 1988.

PSAS: A Quick Derivation relating altitude to air pressure, Portland State Aerospace Society, US, http://psas.pdx.edu/RocketScience/PressureAltitude_Derived.pdf, 2004.

Randel, W. J., Wu, F., and Gaffen, D. J.: Interannual variability of the tropical tropopause derived from radiosonde data and NCEP reanalyses, Journal of Geophysical Research, 105, 15 509—-15 523, doi:10.1029/2000JD900155, 2000.

Reid, G. C. and Gage, K. S.: Interannual variations in the height of the tropical tropopause, Journal of Geophysical Research, 90, 5629–5635, doi:10.1029/JD090iD03p05629, 1985.

Resmi, E., Mohanakumar, K., and Appu, K.: Effect of polar sudden stratospheric warming on the tropical stratosphere and troposphere and its surface signatures over the Indian region, Journal of Atmospheric and Solar-Terrestrial Physics, 105-106, 15–29, doi:10.1016/j.jastp.2013.07.003, 2013.

Rienecker, M. M., Suarez, M. J., Todling, R., Bacmeister, J., Takacs, L., Liu, H. C., Gu, W., Sienkiewicz, M., Koster, R. D., Gelaro, R., Stajner, I., and Nielsen, J. E.: The GEOS-5 Data Assimilation System—Documentation of versions 5.0.1, 5.1.0, and 5.2.0, NASA Technical Report Series on Global Modeling and Data Assimilation Vol. 27, NASA/TM–2008–104606, NASA Center for AeroSpace Information, Maryland, US, 2008.

Rienecker, M. M., Suarez, M. J., Gelaro, R., Todling, R., Bacmeister, J., Liu, E., Bosilovich, M. G., Schubert, S. D., Takacs, L., Kim, G. K., Bloom, S., Chen, J., Collins, D., Conaty, A., da Silva, A., Gu, W., Joiner, J., Koster, R. D., Lucchesi, R., Molod, A., Owens, T., Pawson, S., Pegion, P., Redder, C. R., Reichle, R., Robertson, F. R., Ruddick, A. G., Sienkiewicz, M., and Woollen, J.: MERRA: NASA's Modern-Era Retrospective Analysis for Research and Applications, J. Climate, 24, 3624–3648, doi:10.1175/JCLI-D-11-00015.1, 2011.

Rocken, C., Anthes, R., Exner, M., Hunt, D., Sokolovskiy, S., Ware, R., Gorbunov, M., Schreiner, W., Feng, D., Herman, B., Kuo, Y.-H., and Zou, X.: Analysis and validation of GPS/MET data in the neutral atmosphere, Journal of Geophysical Research, 102, 29 849—-29 866, doi:10.1029/97JD02400, 1997.

Saji, N. H., Goswami, B. N., Vinayachandran, P. N., and Yamagata, T.: A dipole mode in the tropical Indian Ocean, Nature, 401, 360–363, 1999.

Santer, B. D., Wehner, M. F., Wigley, T. M. L., R., Meehl, G. A., Taylor, K. E., Ammann, C., Arblaster, J., Washington, W. M., Boyle, J. S., and Brüggemann, W.: Contributions of Anthropogenic and Natural Forcing to Recent Tropopause Height Changes, Current Science, 301, 479–483, doi:10.1126/science.1084123, 2003a.

Santer, B. D., Sausen, Wigley, T. M. L., Boyle, J. S., andC. Doutriaux, K. A., Hansen, J. E., Meehl, G. A., Roeckner, E., Ruedy, R., Schmidt, G., and Taylor, K. E.: Behavior of tropopause height and atmospheric temperature in models, reanalyses, and observations: Decadal changes, Journal of Geophysical Research, 108, 4ACL 1–1–ACL 1–22, doi:10.1029/2002JD00225, 2003b.

Santer, B. D., Wigley, T. M. L., Mears, C., Wentz, F. J., Klein, S. A., Seidel, D. J., Taylor, K. E., Thorne, P. W., Wehner, M. F., Gleckler, P. J., Boyle, J. S., Collins, W. D., Dixon, K. W., Doutriaux, C., Free, M., Fu, Q., Hansen, J. E., Jones, G. S., Ruedy, R., Karl, T. R., Lanzante, J. R., Meehl, G. A., Ramaswamy, V., Russell, G., and Schmidt, G. A.: Amplification of Surface Temperature Trends and Variability in the Tropical Atmosphere, Science, 309, 1551–1556, doi:10.1126/science.1114867, 2005.

Santer, B. D., Thorne, P. W., Haimberger, L., Taylor, K. E., Wigley, T. M. L., Lanzante, J. R., Solomon, S., Free, M., Gleckler, P. J., Jones, P. D., Karl, T. R., Klein, S. A., Mears, C., Nychka, D., Schmidt, G. A., Sherwood, S. C., and Wentz, F. J.: Consistency of modelled and observed temperature trends in the tropical troposphere, International Journal of Climatology, 13, 1703–1722, doi:doi:10.1002/joc.1756, 2008.

Sausen, R. and Santer, B. D.: Use of changes in tropopause height to detect human influences on climate, Meteorologische Zeitschrift, 3, 131–136, doi:10.1127/0941-2948/2003/0012-0131, 2003.

Schmidt, T., Wickert, J., Beyerle, G., and Heise, S.: Global tropopause height trends estimated from GPS radio occultation data, Geophysical Research Letters, 35, doi:10.1029/2008GL034012, 2008.

Schmidt, T., Wickert, J., and Haser, A.: Variability of the upper troposphere and lower stratosphere observed with GPS radio occultation bending angles and temperatures, Advances in Space Research, 46, 150–161, doi:10.1016/j.asr.2010.01.021, 2010.

Seidel, D. J. and Randel, W. J.: Variability and trends in the global tropopause estimated from radiosonde data, Journal of Geophysical Research, 111, doi:10.1029/2006JD007363, 2006.

Seidel, D. J., Ross, R. J., Angell, J. K., and Reid, G. C.: Climatological characteristics of the tropical tropopause as revealed by radiosondes, Journal of Geophysical Research, 106, doi:10.1029/2000JD900837, 2001.

Seidel, D. J., Gillett, N. P., Lanzante, J. R., Shine, K. P., and Thorne, P. W.: Stratospheric temperature trends: our evolving understanding, WIREs Climate Change, 2, 592–616, doi:10.1002/wcc.125, 2011.

Sen, P. K.: Estimates of the Regression Coefficient Based on Kendall's Tau, Journal of the American Statistical Association, 63, 1379–1389, doi:10.1080/01621459.1968.10480934, 1968.

Sridharan, S., Raghunath, K., Sathishkumar, S., and Nath, D.: Mie lidar and radiosonde observations at Gadanki (13.5°N, 79.2°E) during sudden stratospheric warming of 2009, Journal of Atmospheric and Solar-Terrestrial Physics, 73, 544–550, doi:10.1016/j.jastp.2010.11.016, 2011.

Steiner, A. K., Lackner, B. C., Ladstädter, F., Scherllin-Pirscher, B., Foelsche, U., and Kirchengast, G.: GPS radio occultation for climate monitoring and change detection, Radio Science, 46, doi:10.1029/2010RS004614, 2011.

Steiner, A. K., Hunt, D., Ho, S.-P., Kirchengast, G., Mannucci, A. J., Scherllin-Pirscher, B., Gleisner, H., von Engeln, A., Schmidt, T., Ao, C., Leroy, S. S., Kursinski, E. R., Foelsche, U., Gorbunov, M., Heise, S., Kuo, Y.-H., Lauritsen, K. B., Marquardt, C., Rocken, C., Schreiner, W., Sokolovskiy, S., Syndergaard, S., and Wickert, J.: Quantification of structural uncertainty in climate data records from GPS radio occultation, Atmos. Chem. Phys, 13, 1469—-1484, doi:10.5194/acp-13-1469-2013, 2013.

Sun, B., Reale, A., J., D., and Hunt, D. C.: Comparing radiosonde and COSMIC atmospheric profile data to quantify differences among radiosonde types and the effects of imperfect collocation on comparison statistics, Journal of Geophysical Research, 115, doi:10.1029/2010JD014457, 2010.

Thorne, P. W., Brohan, P., Titchner, H. A., McCarthy, M. P., Sherwood, S. C., Peterson, T. C., Haimberger, L., Parker, D. E., Tett, S. F. B., Santer, B. D., Fereday, D. R., , and Kennedy, J. J.: A quantification of uncertainties in historical tropical tropospheric temperature trends from radiosondes, Journal of Geophysical Research, 116, doi:10.1029/2010JD015487, 2013.

Trenberth, K. E.: Recent Observed Interdecadal Climate Changes in the Northern Hemisphere, Bull. Amer. Meteor. Soc., 71, 988–993, doi:10.1175/1520-0477(1990)071<0988:ROICCI>2.0.CO;2, 1990.

Ware, R., Rocken, C., Solheim, F., Exner, M., Schreiner, W., Anthes, R., Feng, D., Herman, B., Gorbunov, M., Sokolovskiy, S., Hardy, K., Kuo, Y., Zou, X., Trenberth, K., Meehan, T., Melbourne, W., and Businger, S.: GPS Sounding of the Atmosphere from Low Earth Orbit: Preliminary Results, Bull. Amer. Meteor. Soc., 77, 19–40, doi:10.1175/1520-0477(1996)077<0019:GSOTAF>2.0.CO;2, 1996.

Wickert, J., Reigber, C., Beyerle, G., König, R., Marquardt, C., Schmidt, T., Grunwaldt, L., Galas, R., Meehan, T. K., Melbourne, W. G., and Hocke, K.: Atmosphere sounding by GPS radio occultation: First results from CHAMP, Geophysical Research Letters, 28, 29 849–29 866, doi:10.1029/2001GL013117, 2001.

Wickert, J., Michalak, G., Schmidt, T., Beyerle, G., Cheng, C. Z., Healy, S. B., Heise, S., Huang, C. Y., Jakowski, N., Kohler, W., Mayer, C., Offiler, D., Ozawa, E., Pavelyev, A. G., Rothacher, M., Tapley, B., and Arras, C.: GPS Radio Occultation: Results from CHAMP, GRACE and FORMOSAT-3/COSMIC, Terr. Atmos. Ocean. Sci., 20, 35–50, doi:10.3319/TAO.2007.12.26.01(F3C), 2009.

Wilcox, L. J., Hoskins, B. J., and Shine, K. P.: A global blended tropopause based on ERA data. Part II: Trends and tropical broadening, Journal of Geophysical Research, 138, 576–584, doi:10.1002/qj.910, 2011.

WMO: Meteorology - A three-dimensional science: Second session of the commission for aerology, WMO Bulletin, IV, 134–138, 1957.

Zhang, M. L., Liu, L., Wan, W., and B, . N.: An update global model of hmF2 from values estimated from ionosonde and COSMIC/FORMOSAT-3 radio occultation, Advances in Space Research, 53, 395–402, doi:10.1016/j.asr.2013.11.053, 2014.

Zhang, X. and Srinivasan, R.: GIS-based spatial precipitation estimation: a comparison of geostatistical approaches, Journal of the American Water Resources Association, 45, 894—906, doi:10.1111/j.1752-1688.2009.00335.x, 2009.

Table 1. Correlation coefficients between ocean-atmospheric climate indices and temperature anomalies at 200 hPa, 100 hPa, 70 hPa, and 50 hPa for the period August 2006 to December 2013.

Pressure Levels	ENSO		IOD		QBO	
	Correlation	Lag (months)	Correlation	Lag (months)	Correlation	Lag (months)
200 hPa	-0.70	0	-0.42	0	0.39	26
100 hPa	0.82	1	0.27	2	0.47	27
70 hPa	0.40	3	-0.35	-4	-0.45	25
50 hPa	0.27	1	0.34	2	0.53	12

Table 2. Trends in temperature (°C) at 200 hPa, 100 hPa, 70 hPa, and 50 hPa for the period August 2006 to December 2013.

Pressure Levels	COSMIC	MERRA	ERA-Interim
200 hPa	0.02±0.02	0.03±0.03	0.03±0.05
100 hPa	-0.04±0.05	0.00±0.00	-0.02±0.04
70 hPa	-0.07±0.05	-0.04±0.05	-0.05±0.05
50 hPa	-0.02±0.04	-0.01±0.01	-0.01±0.02

Table 3. Trends in tropopause parameters (temperature and height) based on the area-averaged time-series anomalies derived from COSMIC RO and MERRA. Data span between August 2006 and December 2013.

Data	Temperature (°C)	Height (meters)
COSMIC RO	−0.039±0.05	6.01±5.02
MERRA	−0.005±0.03	17.00±10.20

Table 4. Correlation coefficients between tropopause parameters (temperature and height) derived from COSMIC RO and MERRA and ocean-atmospheric indices for the period August 2006 to December 2013.

Data	COSMIC RO		MERRA	
	Temperature	Height	Temperature	Height
Nino3.4 & PC 1	0.77	-0.74	0.78	-0.75
IOD & PC 1	0.35	0.37	0.35	0.38
QBO & PC 2	0.36	0.36	0.53	0.54

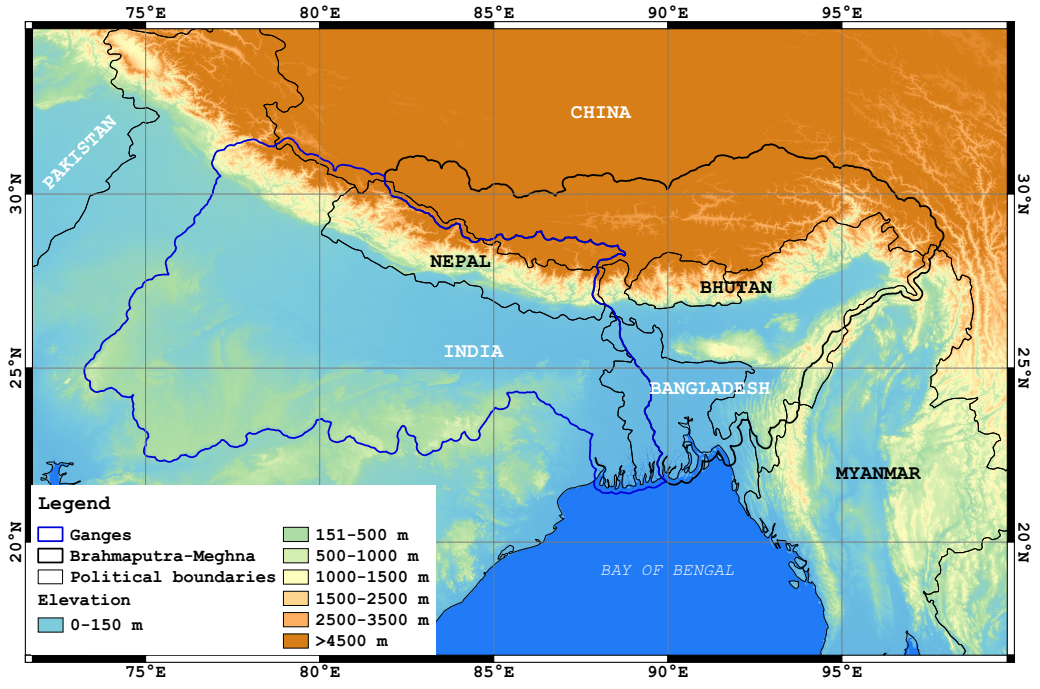

Figure 1. Elevation of the Ganges-Brahmaputra-Meghna Basin in South Asia. The digital elevation model is derived from the Shuttle Radar Topography mission (SRTM, http://srtm.csi.cgiar.org). The locations of the existing radiosonde stations are are shown in circles (black).

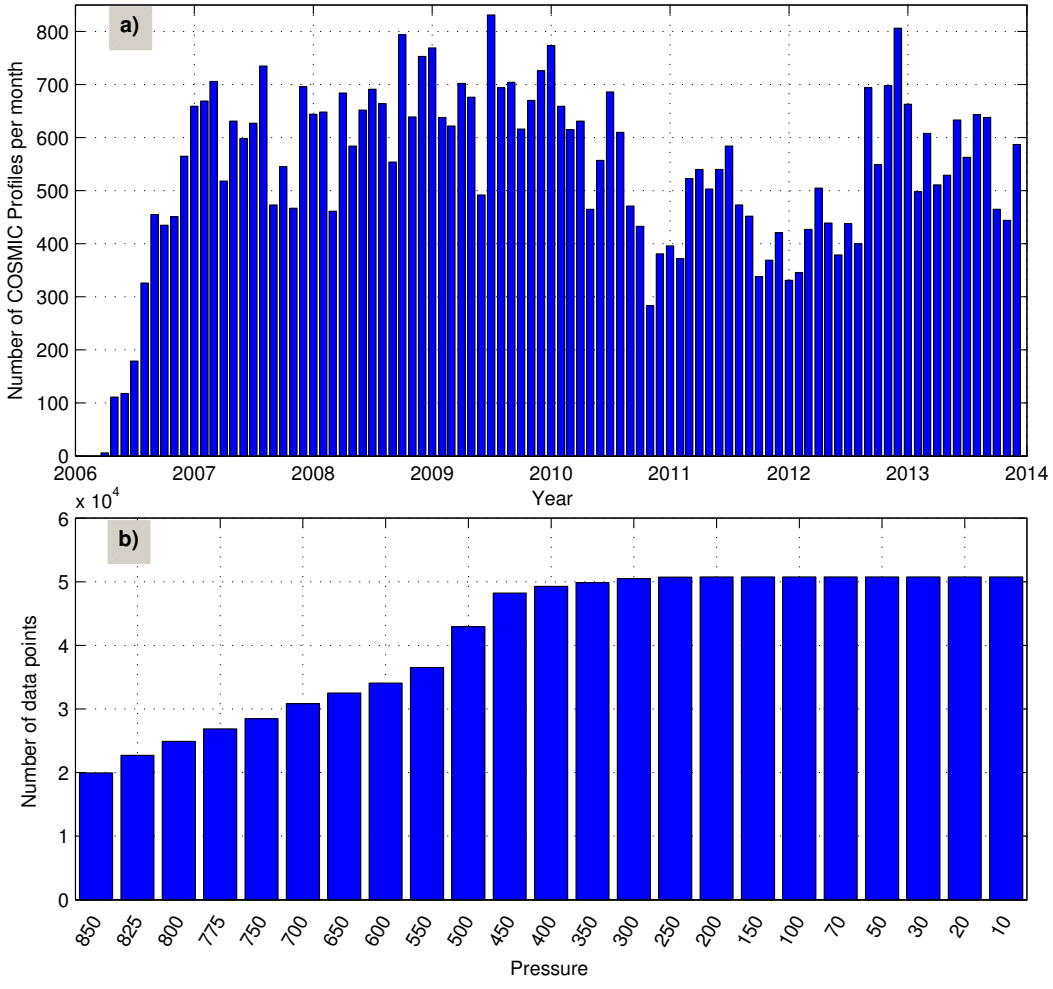

Figure 2. a) Total number of monthly COSMIC RO profiles reported in and around the GBM basin between April 2006 and December 2013, and b) the corresponding number of data points at each pressure levels 850-30 hPa (1.5-24.0 km).

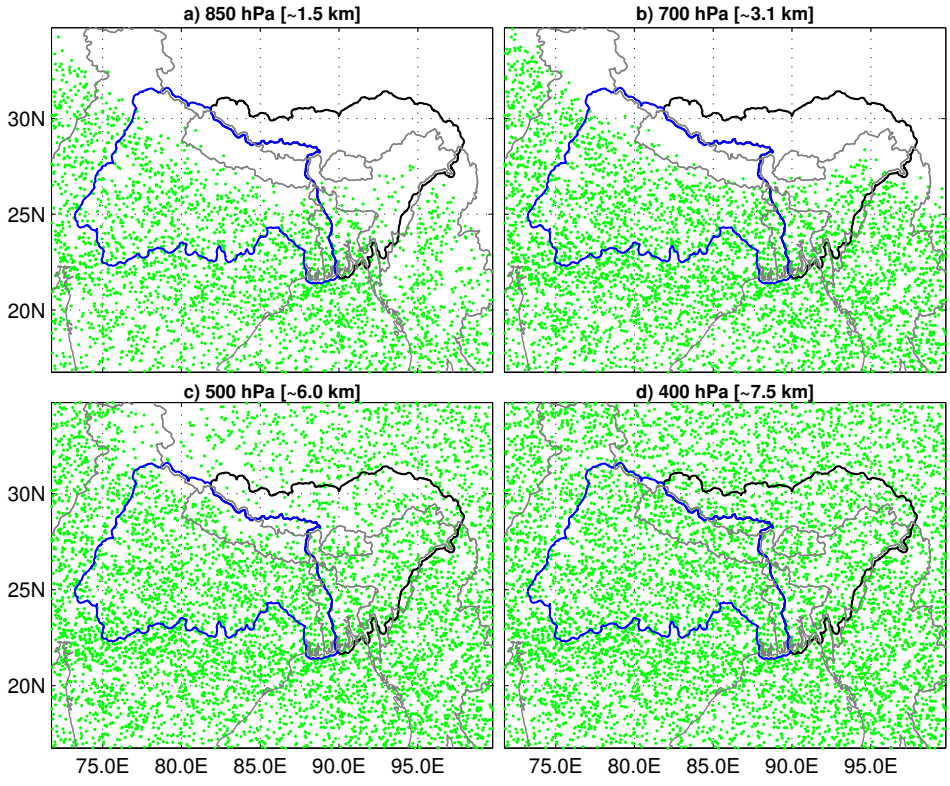

Figure 3. a) Spatial distribution of COSMIC data points in the lower troposphere for the year 2012: a) 850 hPa (∼1.5 km), b) 700 hPa (∼3.1 km), c) 500 hPa (∼5.8 km), and d) 400h Pa (∼7.5 km).

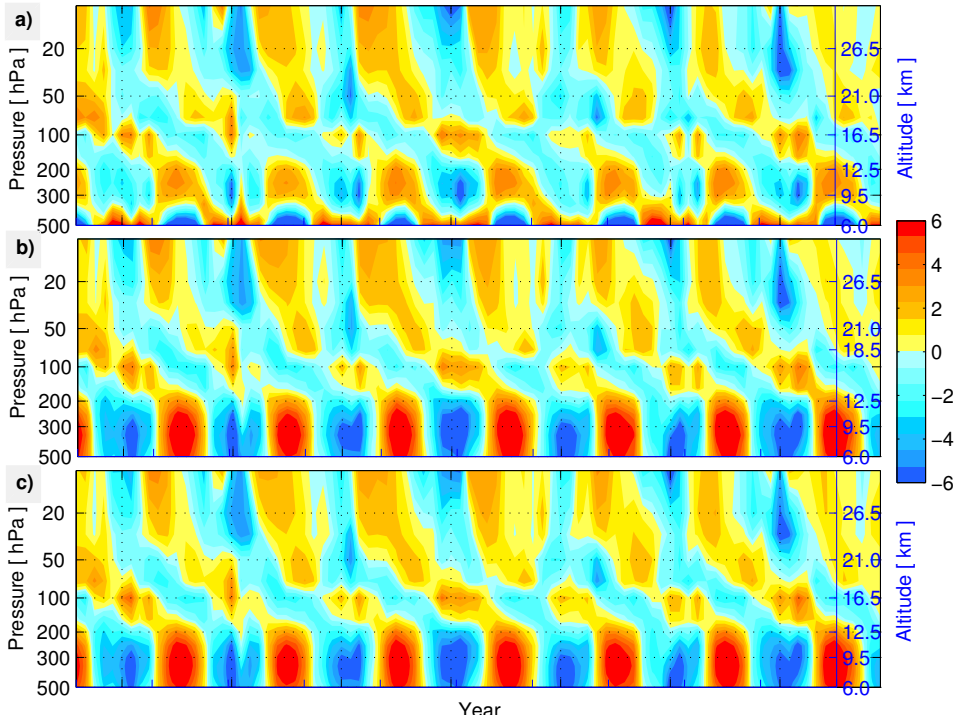

Figure 4. Temporal evolution of temperature(°C) with the time mean removed at each pressure level (500-10 hPa) based on (a) COSMIC RO, (b) MERRA, and (c) ERA-Interim. Data spans between August 2006 and December 2013 and contains area-weighted average over the region (16°N-35°N, 71°E-100°E) covering the GBM basin.

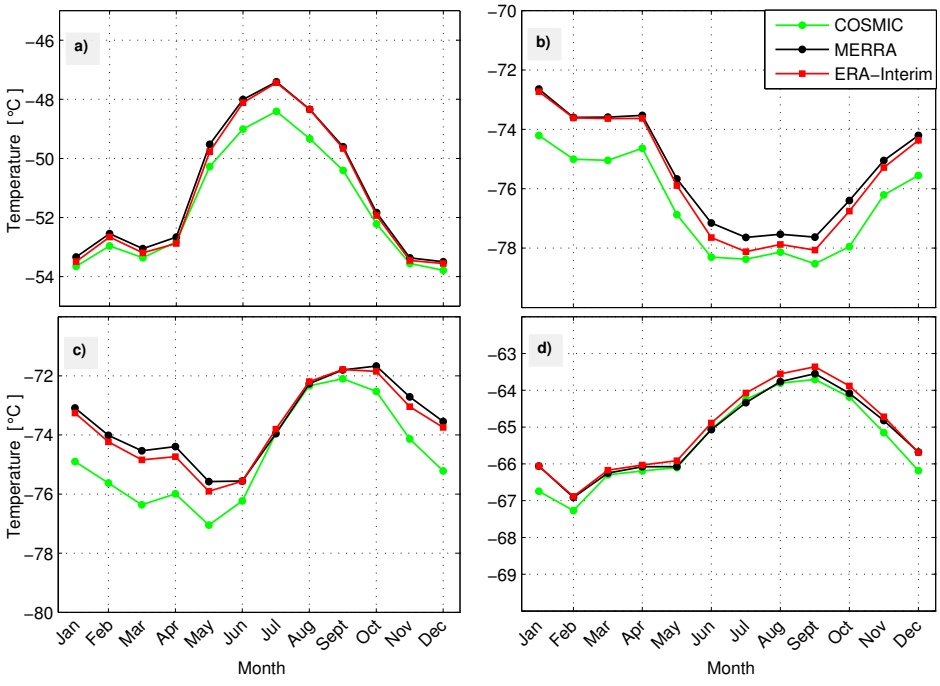

Figure 5. Seasonal cycle of temperature(°C) at (a) 200 hPa, (b) 100 hPa, (c) 70 hPa, and (d) 50 hPa from August 2006 to December 2013 based on COSMIC RO, MERRA, and ERA-Interim averaged over the GBM basin.

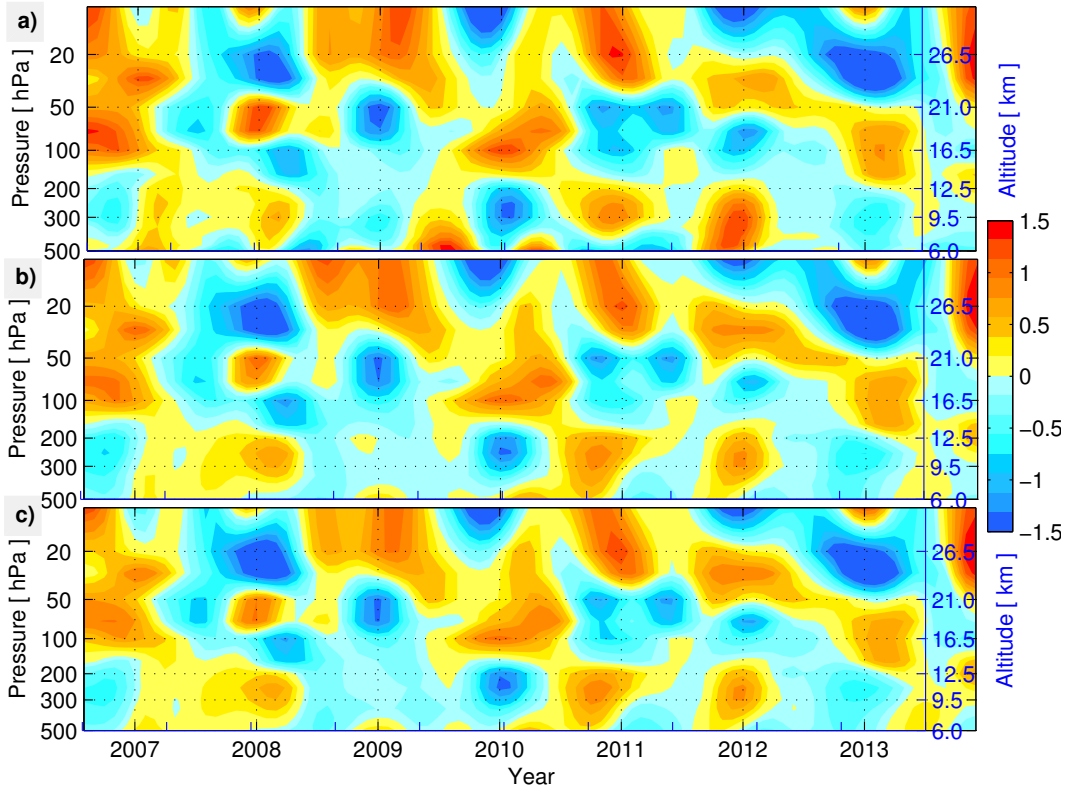

Figure 6. Interannual variability of temperature (°C) in the UTLS region based on (a) COSMIC RO, (b) MERRA, and (c) ERA-Interim from August 2006 to December 2013.

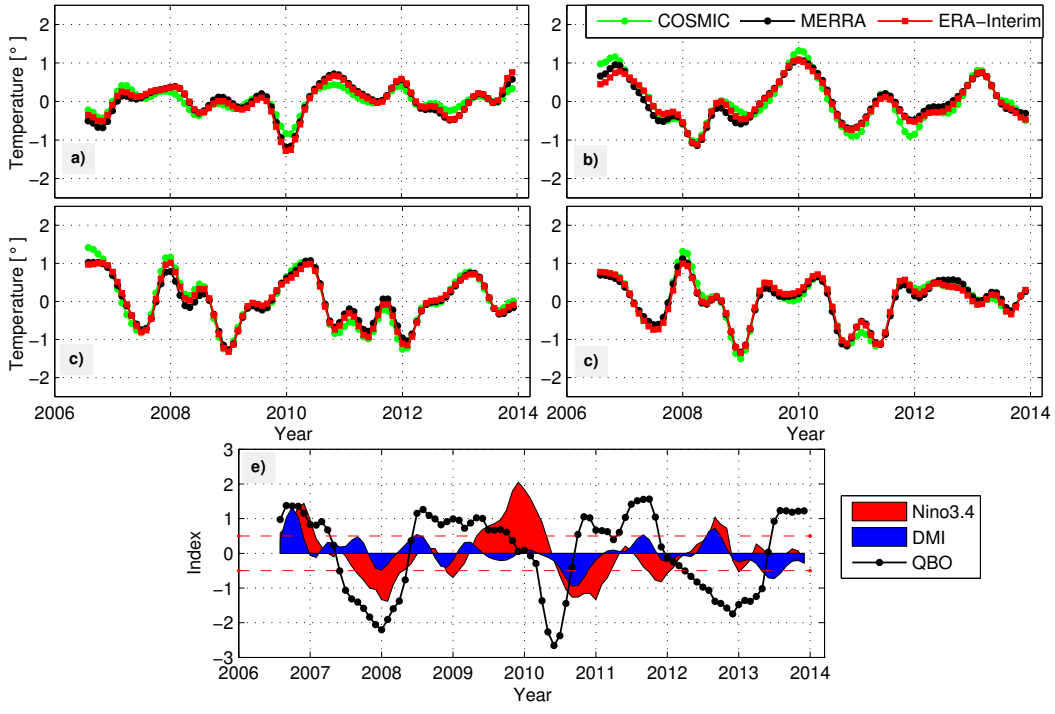

Figure 7. Interannual variability of temperature (°C) at (a) 200 hPa, (b) 100 hPa, (c) 70 hPa, and (d) 50 hPa from August 2006 to December 2013 based on COSMIC RO, MERRA, and ERA-Interim. (e) Ocean-atmospheric indices: Niño3.4, DMI, and QBO are also plotted for reference.

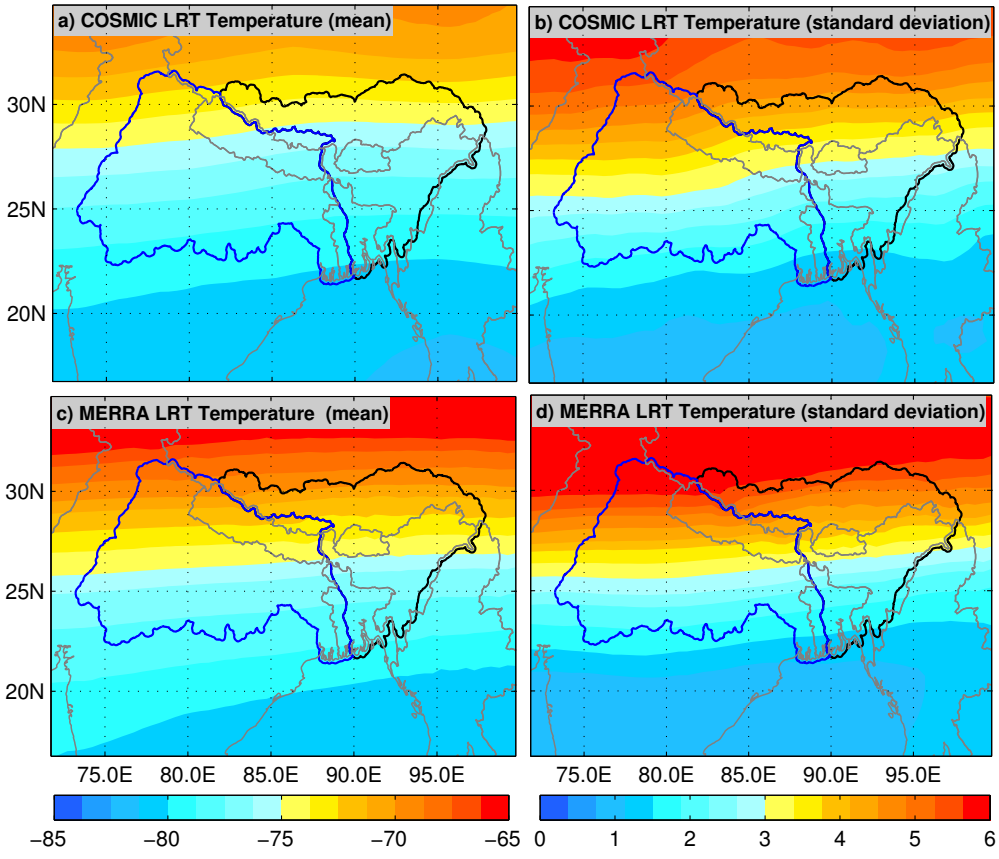

Figure 8. Spatial variation of mean and standard deviation of tropopause temperatures (°C) derived from COSMIC RO and MERRA product based on 89 months from August 2006 to December 2013. (a) Mean and (b) standard deviation of tropopause temperatures (°C) from COSMIC RO, (c) mean and (d) standard deviation of tropopause temperatures (°C) from MERRA product.

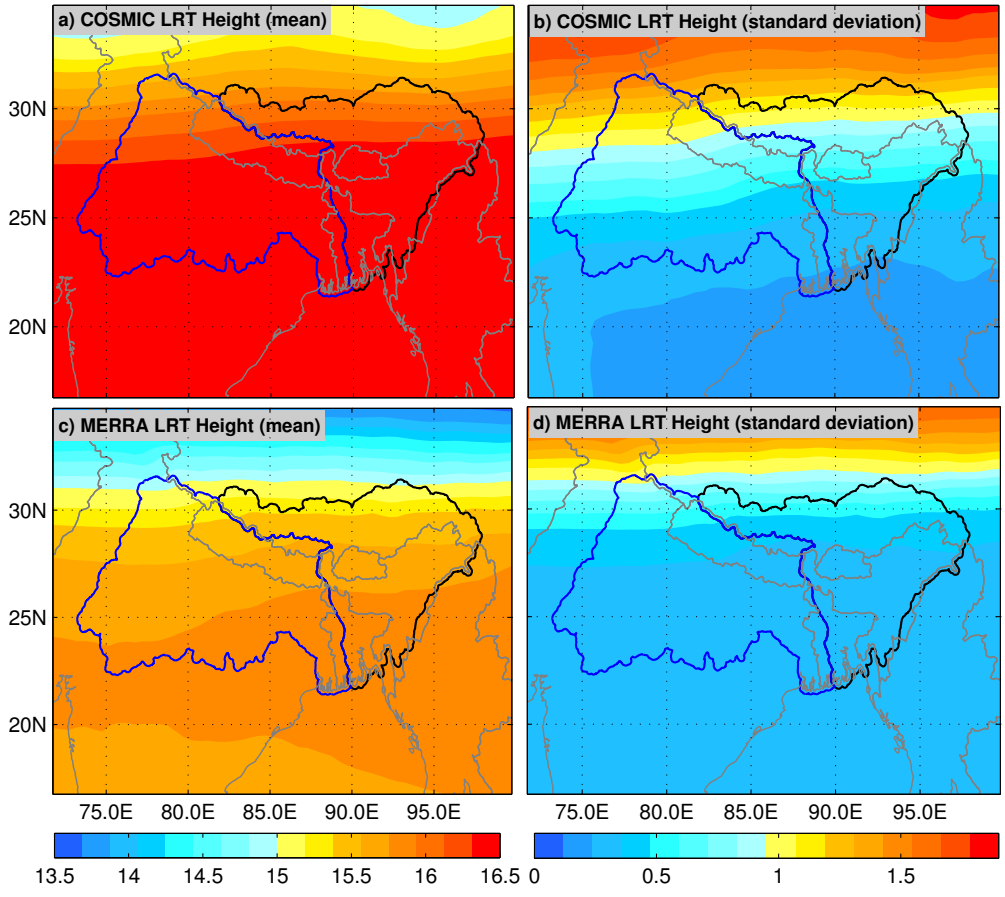

Figure 9. Spatial variation of mean and standard deviation of tropopause heights (km) derived from COSMIC RO and MERRA product based on 89 months from August 2006 to December 2013. (a) Mean and (b) standard deviation of tropopause heights (km) from COSMIC RO, (c) mean and (d) standard deviation of tropopause heights (km) from MERRA product.

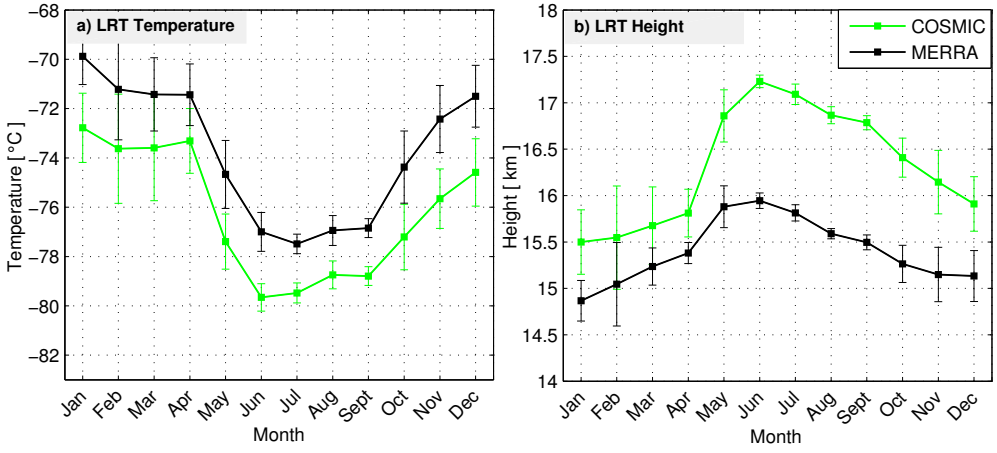

Figure 10. Annual cycle of tropopause over the GBM basin computed from MERRA and COSMIC RO data for the period between August 2006 and December 2013: a) tropopause temperatures, and b) tropopause heights.

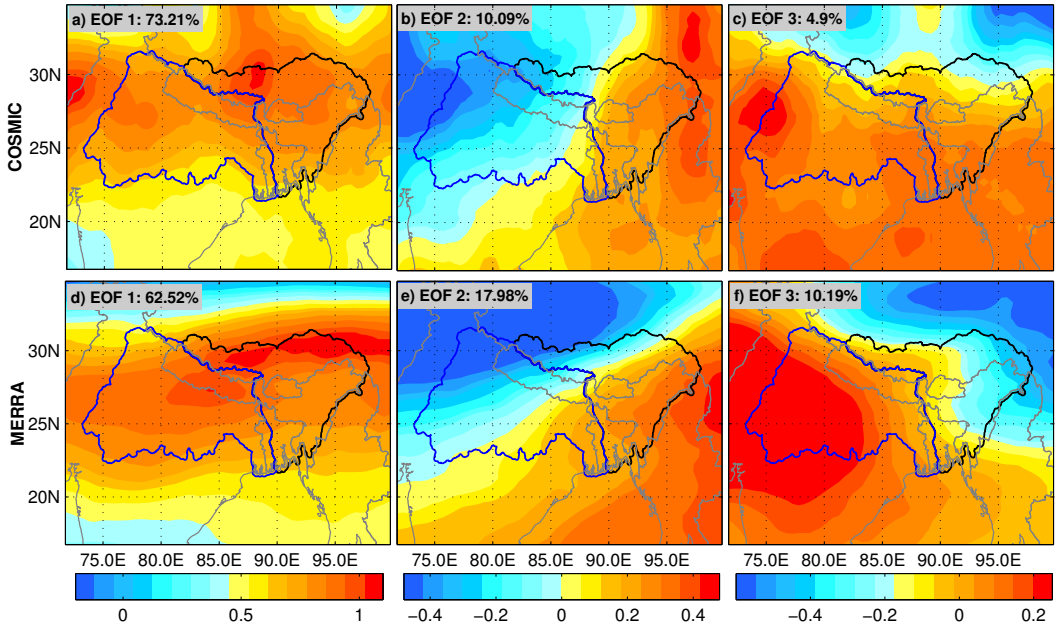

Figure 11. The first three leading EOFs of tropopause temperature (°C) based on MERRA data and COSMIC RO data for the period August 2006 to December 2013.

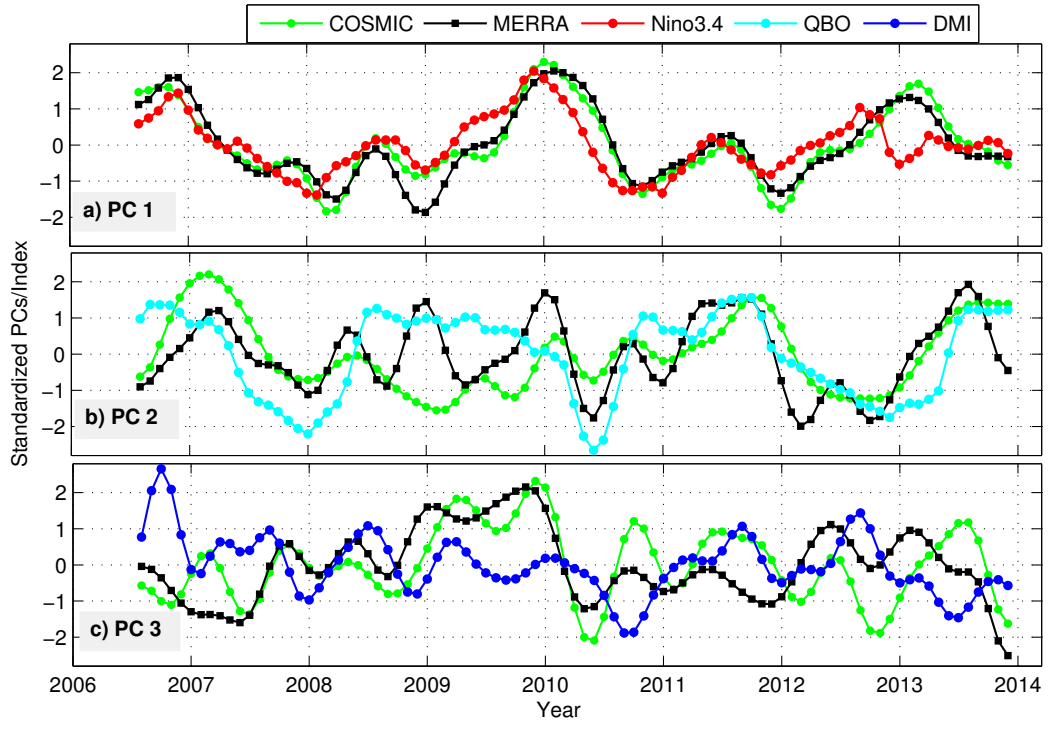

Figure 12. The corresponding PCs (temporal components) based on the three leading orthogonal modes shown in Figure 11.

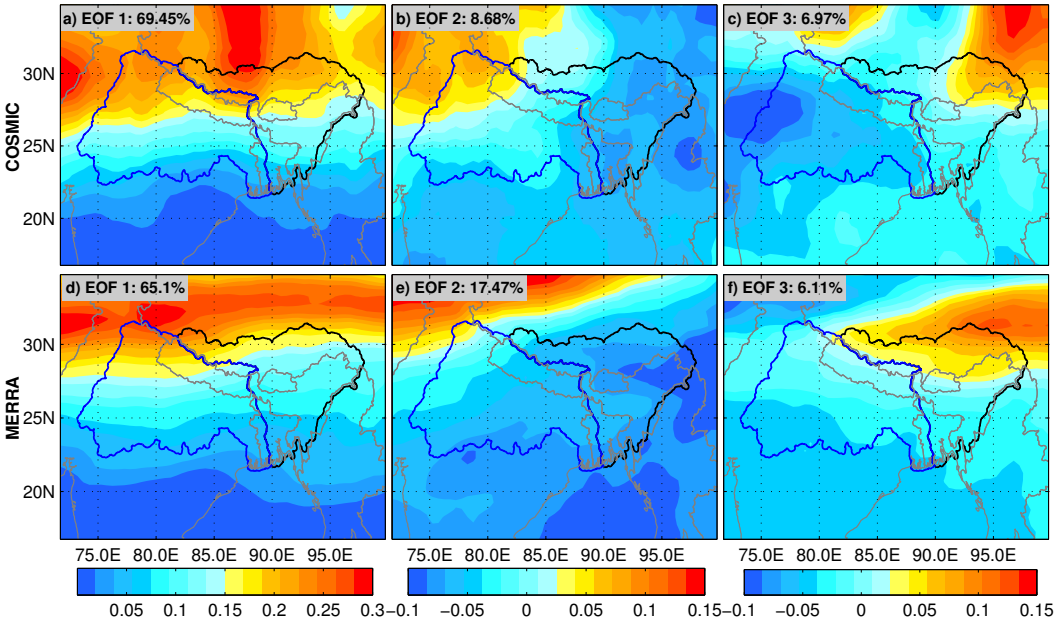

Figure 13. The first three leading EOFs of tropopause height (km) based on MERRA data and COSMIC RO data for the period August 2006 to December 2013.

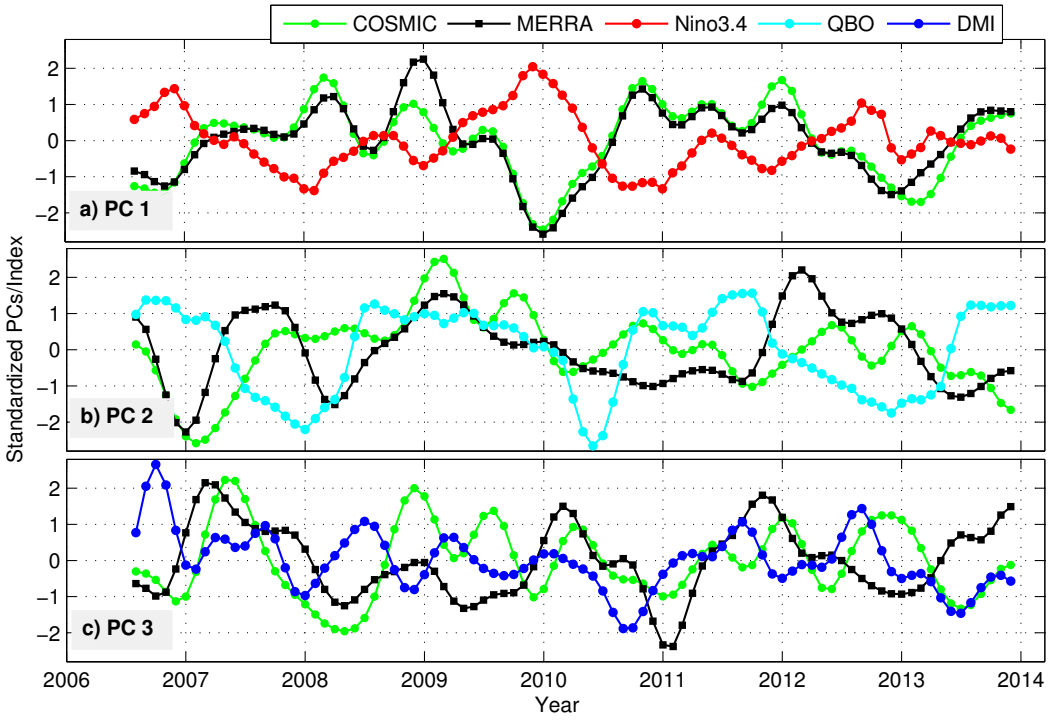

Figure 14. The corresponding PCs (temporal components) based on the three leading orthogonal modes shown in Figure 13.

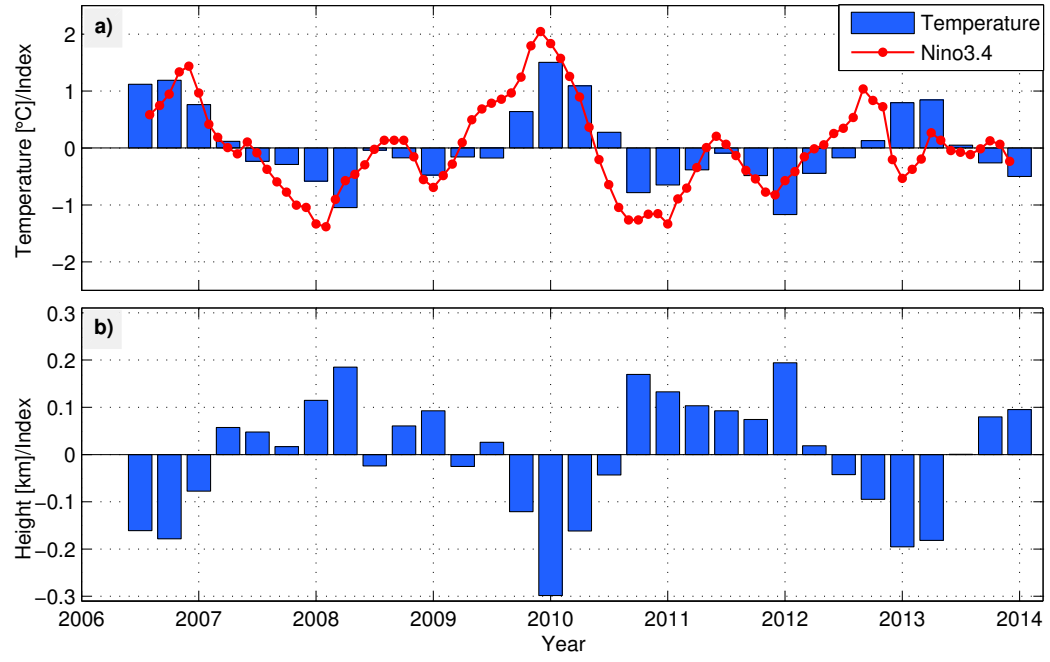

Figure 15. Seasonal mean tropopause temperature and height anomalies due to ENSO mode together with the Niño3.4 index. The area-averaged time series were obtained by multiplying EOF 1 and PC 1, i.e., basically showed the replication of ENSO mode.